SALT CRUST, BRINE, AND MARGINAL GROUNDWATER OF GREAT SALT LAKE'S NORTH ARM (2019 TO 2021)

by Elliot Jagniecki, Andrew Rupke, Stefan Kirby, and Paul Inkenbrandt

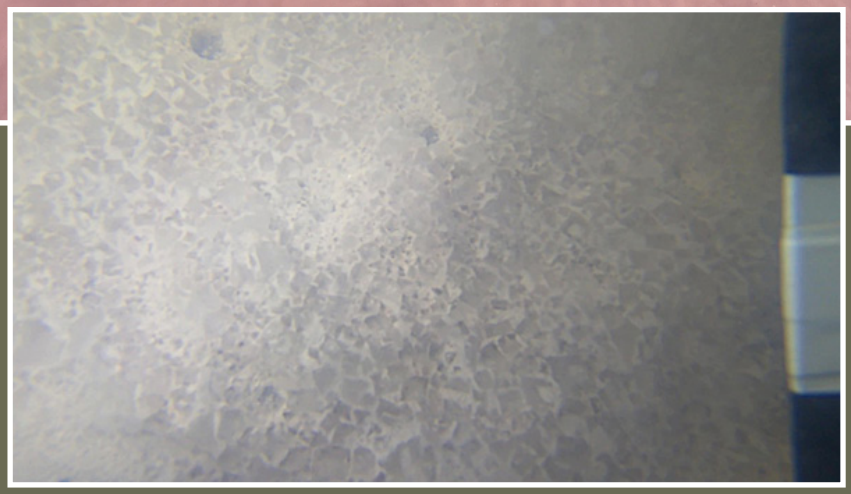

REPORT OF INVESTIGATION 283
UTAH GEOLOGICAL SURVEY
UTAH DEPARTMENT OF NATURAL RESOURCES
2021

Blank pages are intentional for printing purposes.

SALT CRUST, BRINE, AND MARGINAL GROUNDWATER OF GREAT SALT LAKE'S NORTH ARM (2019 TO 2021)

by Elliot Jagniecki, Andrew Rupke, Stefan Kirby, and Paul Inkenbrandt

Cover photo: *North arm lake brine near the Spiral Jetty with wave rippled halite crust (view is to the north).*

Inset photo: *Underwater photograph of the Great Salt Lake north arm lake bottom salt crust at a water depth of 19 ft. The image shows bottom growth cubic halite crystals and circular dissolution pipes. Scale bar is in inches. Near site LVG4; May 25, 2021.*

Suggested citation:

Jagniecki, E., Rupke, A., Kirby, S., and Inkenbrandt, P., 2021, Salt crust, brine, and marginal groundwater of Great Salt Lake's north arm (2019 to 2021): Utah Geological Survey Report of Investigation 283, 40 p., 4 appendices, https://doi.org/10.34191/RI-283.

REPORT OF INVESTIGATION 283
UTAH GEOLOGICAL SURVEY
UTAH DEPARTMENT OF NATURAL RESOURCES
2021

STATE OF UTAH
Spencer J. Cox, Governor

DEPARTMENT OF NATURAL RESOURCES
Brian Steed, Executive Director

UTAH GEOLOGICAL SURVEY
R. William Keach II, Director

PUBLICATIONS
contact
Natural Resources Map & Bookstore
1594 W. North Temple
Salt Lake City, UT 84116
telephone: 801-537-3320
toll-free: 1-888-UTAH MAP
website: utahmapstore.com
email: geostore@utah.gov

UTAH GEOLOGICAL SURVEY
contact
1594 W. North Temple, Suite 3110
Salt Lake City, UT 84116
telephone: 801-537-3300
website: geology.utah.gov

CONTENTS

FIGURES

TABLES

SALT CRUST, BRINE, AND MARGINAL GROUNDWATER OF GREAT SALT LAKE'S NORTH ARM (2019 TO 2021)

by Elliot Jagniecki, Andrew Rupke, Stefan Kirby, and Paul Inkenbrandt

ABSTRACT

Following the construction of the railroad causeway in 1959, a perennial halite (NaCl) bottom crust has been known to exist in the north arm (Gunnison Bay) of Great Salt Lake, Utah, but the lake conditions controlling accumulation or dissolution of the crust are not well defined, including how depth-controlled chemodynamic and hydrodynamic factors influence the degree of the halite saturation. Immediately prior to the opening of a new bridge in the causeway in early December 2016 when north arm lake elevation was at a historical low (just above 4189 feet), the north arm lake brine was at halite saturation. After the opening, inflow of less saline south arm water mixed with north arm water, raised lake elevation, and diluted the north arm lake brine to undersaturation with respect to halite. The following five years have resulted in annual and seasonal fluctuations of halite saturation states. Beginning in mid-2019, the Utah Geological Survey began a study of the north arm to better understand and document the transitions of halite saturation state following the bridge opening using newly collected data as well as reviewing available past data. We investigated the accumulation of salt in the nearshore environment, utilized underwater photography to observe lake bottom salt crust, deployed buoy stations to observe salt accumulation, took water profile measurements, performed density measurements and experiments, and implemented geochemical modeling to understand mineral saturation states. In parallel, groundwater contribution and influence on the salt crust were investigated. Based on our observations and experimentation, we estimate the halite saturation density of the north arm water is approximately 1.223 g/cm^3 at 20°C. Our observations show that the entire north arm water column can reach halite saturation and that coarse halite crystalline growth occurs on the lake bottom in both shallow and deep areas. Using the developed methods, we were also able to observe and document three transitions of saturation state of the north arm brine: 1) halite undersaturation in the second half of 2019 through the first half of 2020 to supersaturated in the second half of 2020, 2) halite undersaturation in very late 2020 through most of the first half of 2021, and 3) halite supersaturation in the late first half of 2021. Although observations are somewhat limited for 2017 and, particularly 2018, 2020 may have been the first season of significant halite precipitation following the bridge opening. Notably, in 2020, the north arm did not reach halite saturation until August, but in 2021 the north arm had already reached saturation by late May, which could be a function of lower lake level, the north arm reaching hydrologic equilibrium following the bridge opening, or both.

Observations and geochemical modeling indicate that groundwater discharge near the lake margins and nearshore environments appears to influence dissolution of the halite crust as well as the inflow of solutes that contribute to the north arm brine chemistry. Springs and seeps are abundant along the lake margin and we observed dissolution of the salt crust at depth in the lake suggesting groundwater input. Modeling of marginal spring water shows that their evaporated brines can evolve to north arm waters, but the extent of their contribution remains unclear. Many of the spring waters pond in various low areas and precipitate carbonate, gypsum, and halite.

Saturation state of the north arm may also be seasonally affected by mirabilite precipitation, which occurs at low temperatures. Laboratory experiments showed that mirabilite precipitation from lake brine can lower salinity suggesting that mirabilite controls north arm undersaturation during winter and spring; however, the relative significance of increased south arm water inflow to the north arm during winter and spring versus mirabilite precipitation is unknown.

INTRODUCTION

Background and Purpose

Understanding the dynamics of the salt cycle and salt balance of Great Salt Lake (GSL) continues to be a challenge and several aspects of the system remain poorly constrained. The salt cycle and balance are important for the lake's ecosystem and industries, both of which hinge on salinity levels. Furthermore, GSL managing agencies and stakeholders need to understand the salt cycle and balance to make informed decisions. The majority of salt within the system resides in solution in the north and south arms of the lake (figure 1) and in a salt, or halite (NaCl) crust in the north arm that fluctuates based on lake and seasonal conditions. In the past, modeling has been used to estimate salt movement between these three primary sinks (or reservoirs) (Loving and others, 2000; Mohammed and Tarboton, 2012) and recent field observations show that nearshore north arm salt crust thickness can fluctuate substantially (± 0.5 ft) on a seasonal basis (Rupke and others, 2016; Rupke and Boden, 2020). However, only limited research has focused on the physical and chemical conditions controlling the cycling of salt between the north arm brine and the north arm salt crust. These conditions serve as a ref-

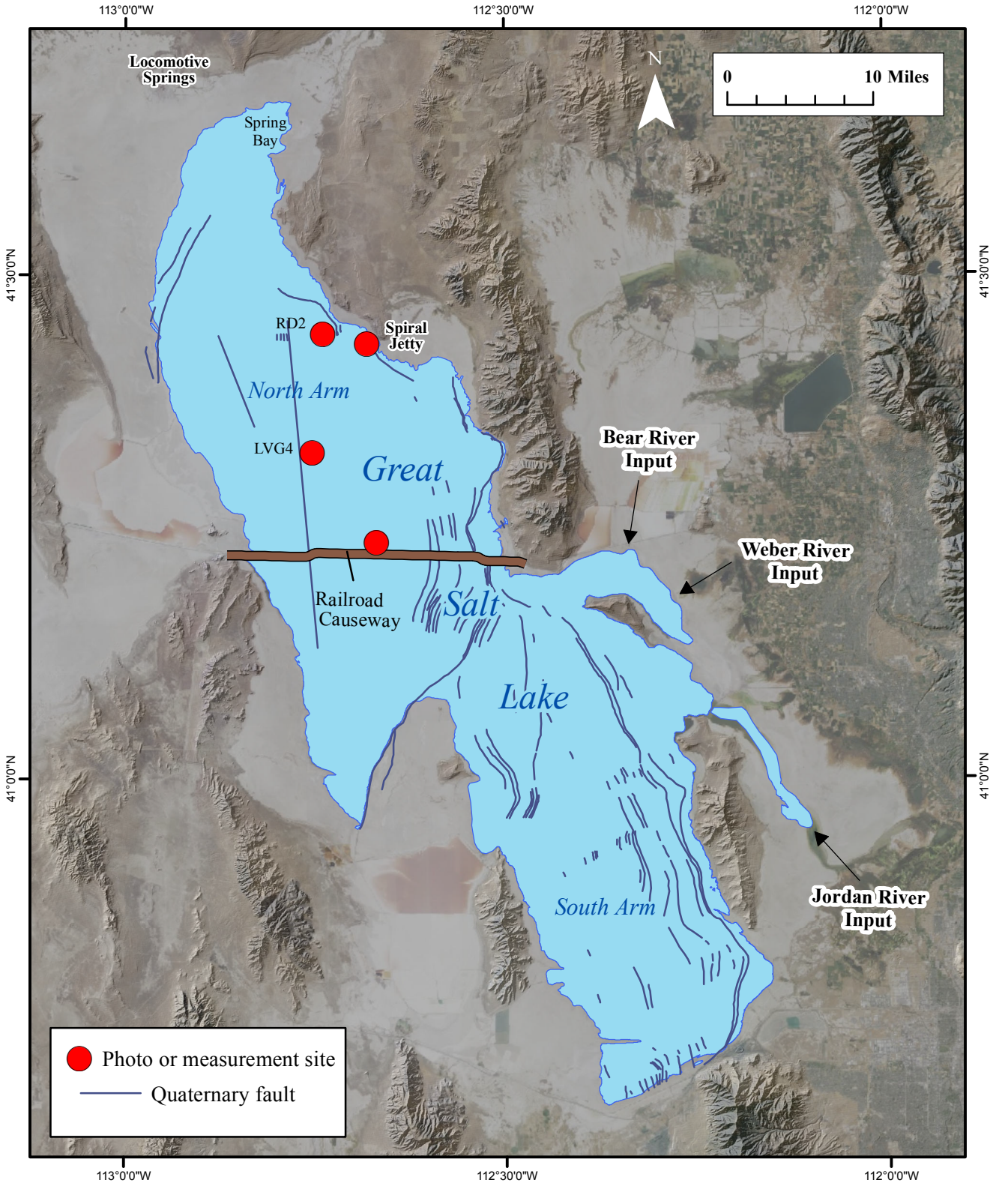

Figure 1. *Great Salt Lake area showing the locations of photography, buoy, observation, and water profile measurement sites. Lake level is represented at 4194 ft above mean sea level. Quaternary faults are from the Utah Geologic Hazards Portal (https://geology.utah.gov/apps/hazards/). Background is 2018 NAIP imagery.*

erence in comparison to how the north arm brine and salt crust has responded to the opening of the new railroad causeway bridge in December 2016.

Past modeling of the lake's salt cycle assumed a closed system with no salt added or removed over time (Loving and others, 2000; Mohammed and Tarboton, 2012). The total salt load used in these models was calculated during the high-water-level years of GSL in the 1980s when the majority of salt was assumed to be in solution. The load was estimated to be roughly 4.5 billion tons following the West Desert Pumping Project (Loving and others, 2000; Mohammed and Tarboton, 2012). However, fluxes of salt into and out of the system may have important effects on the overall salt load and balance. Industry extraction of salt currently withdraws about a million tons from the system each year (Mills and others, 2020), and recent research by Shope and Angeroth (2015) suggests that riverine input of dissolved solids may be more significant than previously thought. Another potentially significant, but less studied, solute input source is groundwater. Research focused on detection of potential groundwater sources in and around the lake could help determine its significance. In addition, it is unknown how density mixing of the less-saline south arm brines with north arm brines is occurring at the breach of the causeway that was opened in December 2016. The impact to the salinity of the north arm due to less-dense south arm water flowing over a denser north arm brine is not well understood. However, recent computational fluid dynamics and artificial neural network modeling has indeed characterized north-to-south, south-to-north, and bidirectional density-driven flow patterns through the breach (Rasmussen and others, 2021).

The overall purpose of this study was to document systematic limno-sedimentological observations and field-laboratory geochemical measurements of the north arm salt system and build upon studies by Rupke and others (2016) and Rupke and Boden (2020) that mostly occurred prior to the late 2016 opening of the causeway bridge. Using new observations and measurements from this study, we hope to better understand 1) what controls halite precipitation and dissolution, 2) how the north arm is responding to the opening of the 2016 causeway bridge, and 3) how potential groundwater discharge at the north arm shore and lake bottom might impact solute balance and halite crust dissolution. This report summarizes two funding phases of work conducted from July 2019 through June 2021 that were provided by the Utah Division of Forestry, Fire and State Lands, Department of Natural Resources.

Brine Evolution and North Arm Salt Crust History

The chemistry of modern GSL is the result of the evaporation of intermountain basin waters of the late Pleistocene freshwater Lake Bonneville (Gilbert, 1890; Scott and others, 1983; Spencer and others, 1985; Oviatt and others, 1992), as well as from the contribution of riverine inflow waters and Na-Cl-enriched mesothermal-hydrothermal groundwaters (Cole, 1982; Spencer and others, 1985; Jones and others, 2009). Evaporation is the only outflow and is dependent on lake area and salinity, both of which are affected by lake volume (Mohammed and Tarboton, 2012) and salt loss retained in sediment pore waters (Spencer and others, 1985). The source of solutes is primarily from the chemical weathering of various bedrock lithologies, lacustrine deposits, and glacial till, with parent constituents consisting of Na^+, SiO_2, HCO_3^-, K^+, Ca^{2+}, Mg^{2+}, SO_4^{2-}, and Cl^-. Today, the inflow of water and solutes is primarily dependent on the three major rivers that contribute around 95% of the inflow into the lake, where the Bear and Weber Rivers account for about 73% of the inflow and the Jordan River accounts for about 22% (Mohammad and Tarboton, 2012). The remaining 5% of water input is a combination of subordinate inflow from Davis Creek (~1%), meteoric precipitation, groundwater, and runoff. The minimum annual groundwater discharge into GSL is estimated to be 3%, which is equivalent to ~92–123 million m^3/year (Arnow and Stephens, 1975), whereas some discharge zones in the south arm have a seepage rate of ~0.8 cm/day (Anderson and others, 2014). During low river inflow and high evaporation, spring waters with high concentrations of solutes may contribute to the drainage system in higher proportions of discharge, particularly hydrothermal spring brines that feed the Malad River tributary system to the north that drain into the Bear River (Spencer and others, 1985) and groundwater seeps around the lake (Anderson and others, 2014; Kirby and others, 2019).

The composition of the major solutes and mixing of all surface and groundwater sources are speculated to eventually evolve to a sodium chloride sulfate brine from evaporative concentration in the terminal basin of GSL (Jones and others, 2009). Figures 2 and 3 show the concept of chemical divides and how GSL closed-basin brine has evolved through time to produce the current lake water chemistry and saturation/precipitation of evaporites, including halite (NaCl), gypsum ($CaSO_4{\cdot}2H_2O$), mirabilite ($Na_2SO_4{\cdot}10H_2O$), and glauberite ($Na_2Ca[SO_4]_2$) (Jones and others, 2009). Figure 2 illustrates how the composition of inflow riverine and groundwater evolve into brines in the Ca-HCO_3-SO_4 system and provides examples for other saline lake systems. Interestingly, the three major rivers are carbonate rich and plot in the Na-Cl-HCO_3-SO_4 field, whereas the majority of spring waters along the north arm shore margins reside in the Na-Cl-SO_4 field that evolve to a GSL brine. Figure 3 is a flow diagram that illustrates the concept of chemical divides and brine evolution for the three major brine types, which are Na-CO_3-Cl (e.g., Lake Magadi, Kenya), Na-Cl-SO_4 (e.g., GSL, Utah), and Na-Ca-Cl_2 (e.g., Dead Sea, Israel). The concept of chemical divides allows researchers to understand evaporative brine evolution for inflow waters that enter a closed lake system. The brine evolution for GSL is as follows. First, undersaturated inflow waters precipitate carbonate (calcite, aragonite, dolomite) at the $CaCO_3$ divide and Ca^{2+}-Mg^{2+} and HCO_3^- are removed in a 1:1 ratio,

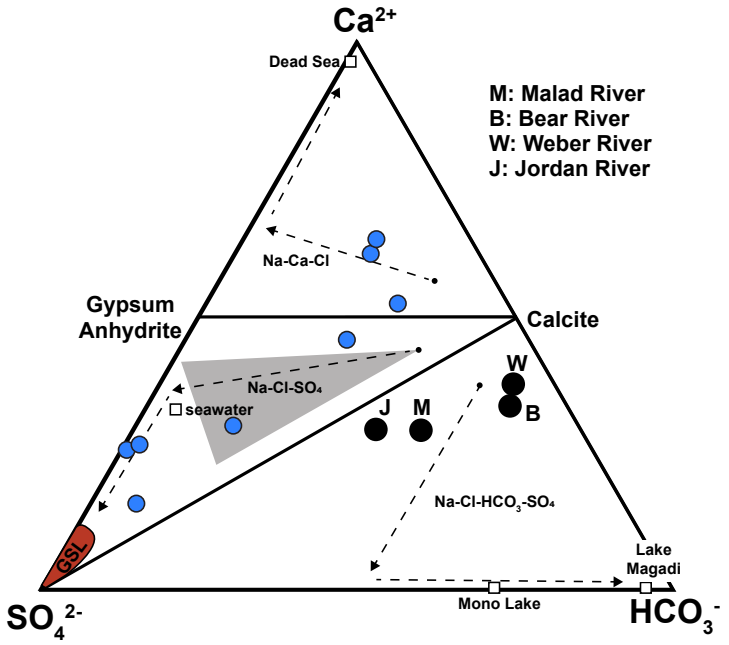

Figure 2. *Ternary phase diagram illustrating how the composition of inflow riverine (large black circles) and lake margin spring waters near Locomotive Springs and Spring Bay (blue circles) (in molar equivalents) evolve into brines in the Ca-HCO_3-SO_4 system. Solid lines show the concept of chemical divides. Lines from calcite to sulfate and calcite to gypsum-anhydrite separate waters that will evolve (dashed lines and arrows) upon evaporation and precipitation of calcite and gypsum into Ca-Cl, Cl-SO_4 , and Na-Cl-HCO_3-SO_4 brines. Brine evolution pathways are dependent on molar equivalents of Ca^{2+}, SO_4^{2-}, and HCO_3^- in inflow waters, which determines the chemical evolution of the brine at the calcite and gypsum/anhydrite chemical divides. Evaporation trend for Great Salt Lake (GSL, red label) begins within the gray shaded area where carbonate (calcite) is first removed, followed by gypsum, and the waters evolve to a sodium chloride sulfate brine. Note the majority of spring waters evolve to a GSL brine. After Jones and others (2009).*

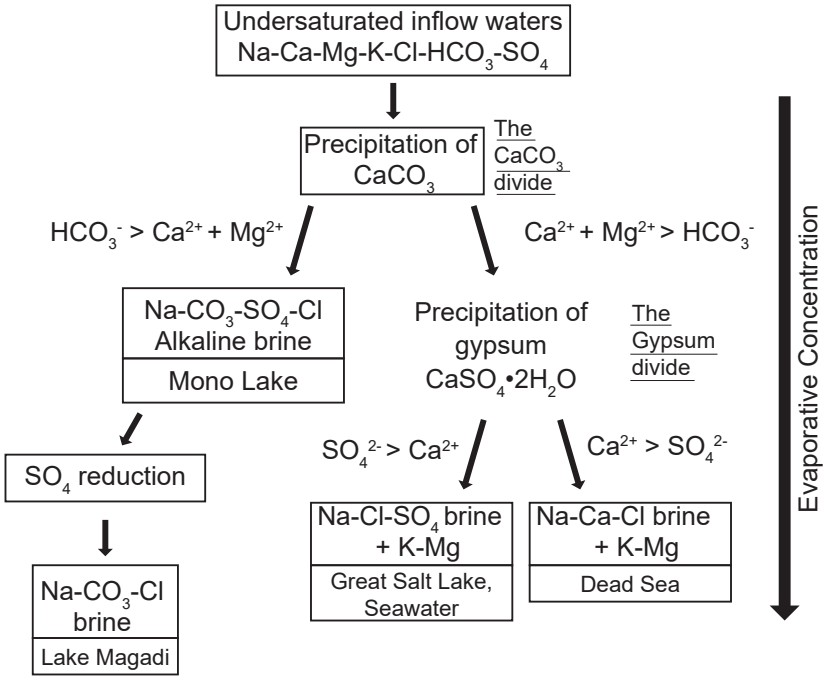

Figure 3. *Flow diagram illustrating the concept of chemical divides and the evolution of three major brine types. All waters precipitate calcite/carbonate first and depending on the remaining molar proportion of Ca^{2+} the brine evolves either into an alkaline brine or a sulfate brine. Mono Lake and Lake Magadi lie on the left side because inflow waters have a low Ca^{2+}/HCO_3^- ratio, whereas Great Salt Lake, seawater, and the Dead Sea lie on the right side because inflow waters have a higher Ca^{2+}/HCO_3^- ratio. After the precipitation of gypsum, the sulfate brine evolves to either a $MgSO_4$ brine (Great Salt Lake, seawater) or a $CaCl_2$ brine (Dead Sea) dependent on SO_4^{2-}/Ca^{2+} ratios. Because Great Salt Lake has relatively high concentrations of SO_4^2, sulfate reduction is not as significant in comparison to bicarbonate-rich Lake Magadi brines that have subordinate amounts of SO_4^{2-} (adapted from Hardie, 2003).*

HCO_3^- becomes depleted, and the brine becomes enriched in SO_4^{2-}. Then the brine approaches the gypsum/anhydrite divide and after precipitation of gypsum the brine becomes depleted in Ca^{2+} and evolves to a Na-Cl-SO_4 brine (figures 2 and 3) (Hardie, 2003). At this point, depending on increasing salinity through evaporative concentration, halite precipitates; extreme evapoconcentration leads to potash (KCl) and magnesium chloride salts. This chemical concept is confirmed by the GSL lake water composition, which is highly depleted in Ca^{2+} and HCO_3^-, and the absence of carbonate or gypsum currently forming within the lake; carbonate precipitates upstream or at spring seeps and gypsum forms along the north arm lakeshore mudflats.

Since the completion of the rock-fill railroad causeway in 1959, a net movement of dissolved solids from the south arm (Gilbert Bay) to the north arm (Gunnison Bay) of GSL has occurred resulting in decreasing dissolved solids (i.e., salinity) in the south arm (figure 4), higher salinity in the north arm, and the precipitation of a halite crust in the north arm (Adams, 1964; Madison, 1970; Goodwin, 1973; Loving and others, 2000; Gwynn, 2002; Gwynn, 2007; Mohammed and Tarboton, 2012; Rupke and McDonald, 2012; Rupke and others, 2016; Utah Geological Survey, 2020). The changes in salinity between the north and south arms is largely a function of limited hydrological connection due to the causeway and that the vast majority of fresh surface inflow enters into the south arm. The causeway was built with only two 15-ft-wide culverts to allow for hydrologic exchange between the north and south arms, but in 1984, a 290-ft-long bridge was constructed on the western end of the causeway to allow elevated south arm water to flow into the north arm. During their lifespan, flow through the culverts was inconsistent and due to structural integrity they were closed in 2012 and 2013. A 180-ft-long bridge was designed and constructed to replace the functionality of the abandoned culverts and that bridge was opened in December 2016.

Observations and modeling indicate that, with the exception of the high water years in the late 1980s and early 1990s,

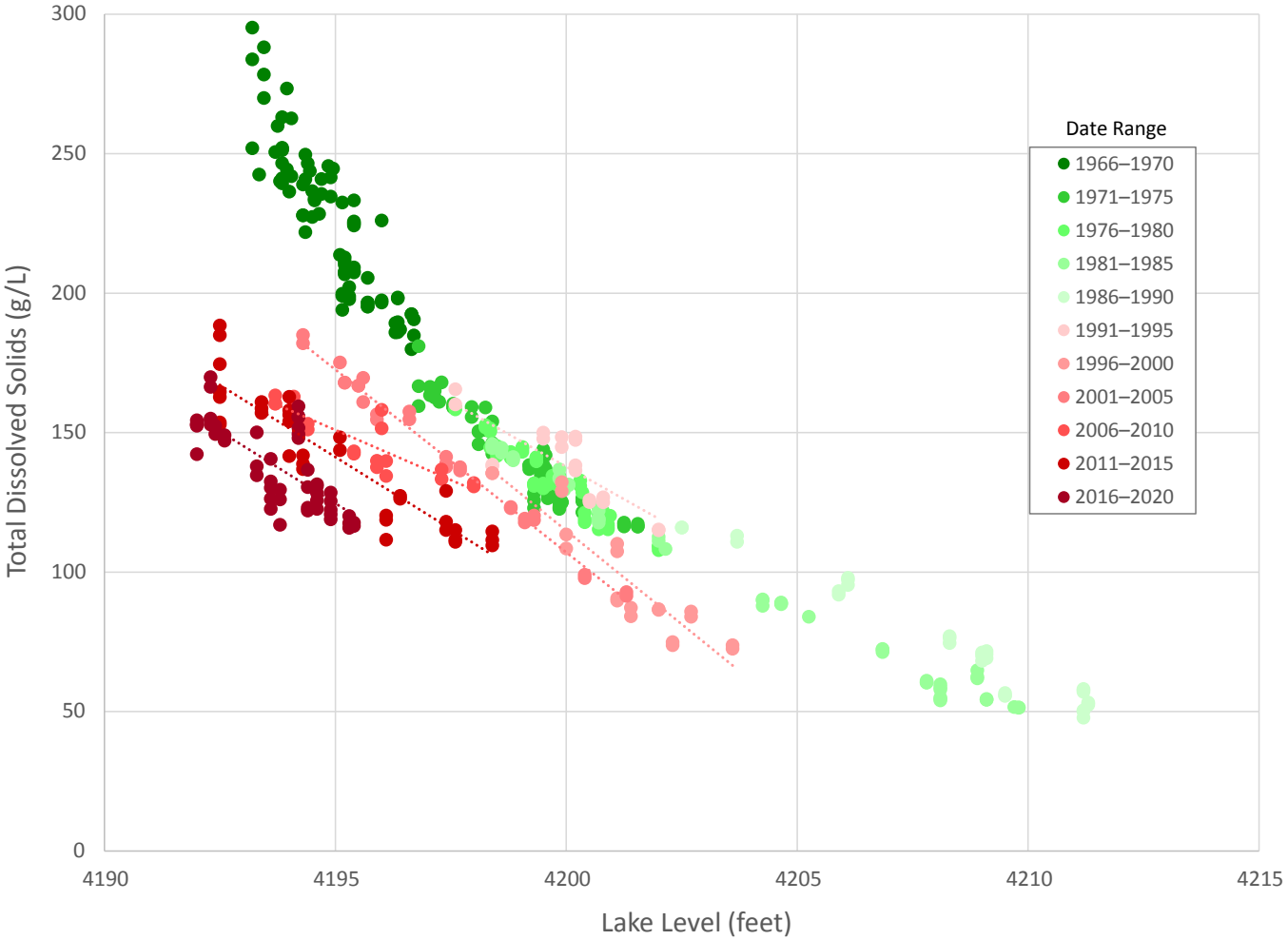

Figure 4. *Great Salt Lake south arm salinity from 1966 to 2020. The data illustrate how the salinity ranges (g/L) of the south arm have decreased over time, particularly from 1996 through 2020. Salinity has an inverse correlation to lake level. The data source is the Utah Geological Survey (2020), and data points are from UGS sample sites AS2, AC3, and FB2 at ~10 feet deep. Trend lines are linear.*

the north arm has been at or close to saturation with respect to halite and a substantial salt crust was present (Loving and others, 2000; Gwynn, 2002; Mohammed and Tarboton, 2012; Utah Geological Survey, 2020). Direct evidence and documentation of the salt crust comes from the early 1970s and the 2010s. In the early 1970s, Goodwin (1973) showed that the salt crust was present throughout the north arm through an extensive drilling program conducted during 1970 and 1972. Woodhall (1980) and Dames and Moore (undated) reported salt crust up to 8 ft thick from a drilling program conducted in the north arm during 1974. No direct documentation is available on the salt crust after 1974 until Rupke and others (2016) and Rupke and Boden (2020) conducted their studies from 2015 through early 2017. Rupke and others (2016) observed a substantial nearshore salt crust (commonly 1 ft thick or more) in several places around the north arm and measured nearshore crust up to nearly 3 ft thick in the northernmost part of the north arm in 2016 (Rupke and Boden, 2020).

Recent observations suggest halite in the north arm primarily forms during the summer and fall (Rupke and others, 2016; Rupke and Boden, 2020). Mirabilite precipitates during the cold winter months due to its stability at low temperatures and gypsum typically forms from interstitial brines along shoreline mudflats during unknown timeframes. Although salt precipitation fluctuates seasonally, particularly as observed in the nearshore (Rupke and others, 2016; Rupke and Boden, 2020), little is known about how the major body of salt crust contained in deeper parts of the north arm changes seasonally or over time and how the precipitation of mirabilite during the winter impacts the degree of halite saturation.

When present, the salt crust is primarily composed of coarsely crystalline halite (Goodwin, 1973; Woodhall, 1980; Rupke and others, 2016). Rupke and others (2016) observed halite growth occurring as fine-grained salt rafts that form on the water surface and coarse idiomorphic bottom growth chevron crystals on the lake floor. Rupke and others' (2016) examination of the crust suggested that salt rafts form at the air-water interface and then sink through the shallow water column, becoming substrate nuclei for the larger, bottom-growth halite crystals (a well-known process previously described by Lowenstein and Hardie [1985] and more recently by Sirota and others [2017] for modern halite deposition in the Dead Sea). Nearshore, the submerged surface of the salt crust was sharp and crystalline during growth seasons (fall and summer) (figure 5) and rounded and planar during dissolution seasons (winter and spring). During Rupke and others' (2016) and Rupke and Boden's (2020) field studies from summer 2015 through spring 2017, substantial salt crust growth was documented (~0.5 ft during the summer and fall), which notably occurred during the lowest historical lake levels recorded in the north arm. Following the initial opening of the new causeway bridge in late 2016, the nearshore crust dissolved and new seasonal growth was minimal in 2017 and 2018.

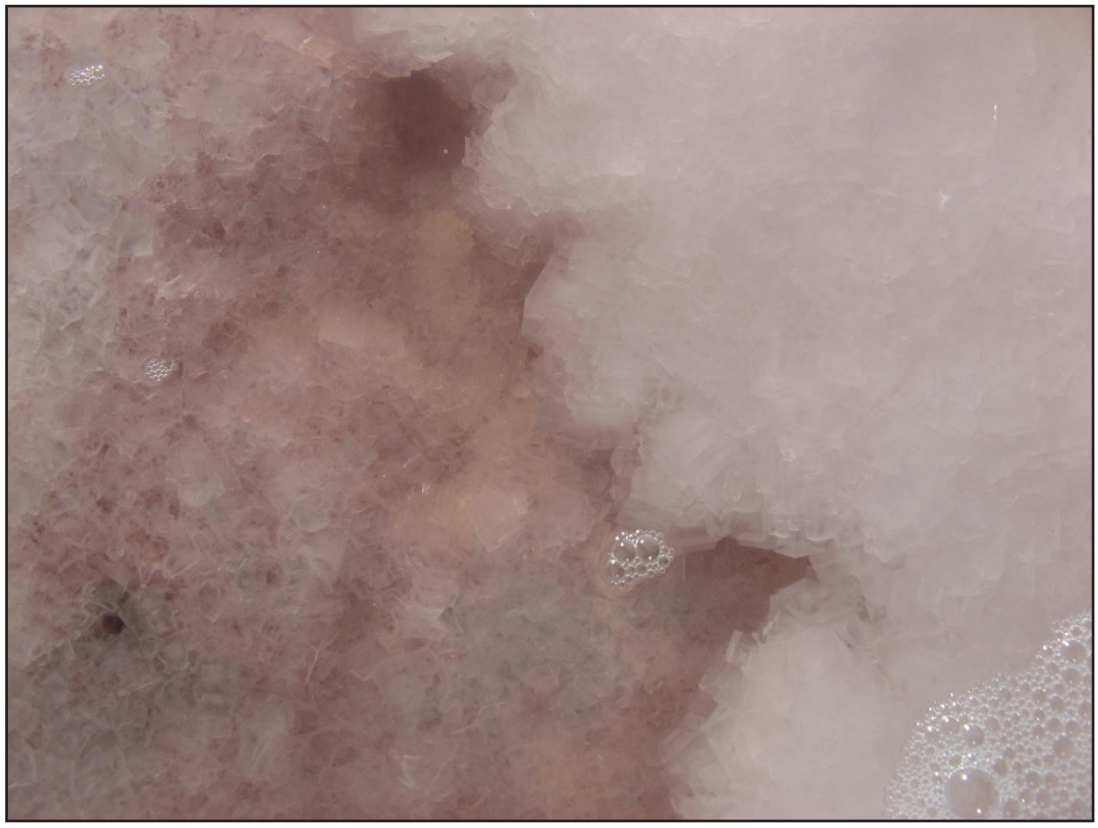

Figure 5. *Submerged coarsely crystalline, newly formed bottom-growth halite crystals. Note coarse texture and sharp crystalline edges. Photograph was taken in late 2015 south of Spiral Jetty. For scale, the bottom edge of the photograph roughly represents about 1 foot.*

Halite Deposition in Saline Lake Basins

Systematic sedimentological and geochemical studies of halite deposition have focused on shallow ephemeral saline playas and deep water hypersaline environments. Shallow saline playas or salt pans such as Badwater Basin, Death Valley, California, typically do not exceed 3 ft (~1 m) of depth after flooding episodes, whereas deep water hypersaline basins can reach up to 1000 ft (~300 m) of depth (e.g., the Dead Sea). Thus, there is a knowledge gap regarding halite accumulation and solute balance in perennial hypersaline basins with intermediate water depths that are capable of seasonal thermohaline stratification (e.g., the north arm of GSL). Halite deposition and dissolution in shallow saline playas or salt pan playas are closely linked to the seasonal hydrologic cycle (Lowenstein and Hardie, 1985; Smoot and Lowenstein, 1991; Bowen and others, 2017; Rupke and Boden, 2020). During the dry summer and early fall seasons, high net evaporation and low water influx result in water level decline and desiccation, accompanied by increased salinity and intensive halite crystallization. In the wet winter and spring season, low net evaporation reduces halite deposition or even dissolves halite crusts when floodwaters and groundwater dilute shallow brines. Each stage of the seasonal cycle is recorded in the textural characteristics of the halite, including dissolution features (pipes, smoothing of crystal tops) produced during the flooding stage and chevron or cornet crystal facies during evapoconcentration (Lowenstein and Hardie, 1985). In deeper brine bodies, the seasonal hydrologic cycle results in smaller salinity variations at depth, and therefore temperature and physico-chemical reactions play an important role in controlling the degree of halite saturation (Sirota and others, 2017). The north arm of GSL, at times, is thermally stratified during the summer and may have no stratification during the winter, and therefore, is an excellent field laboratory for an intermediate depth saline lake. In addition, the precipitation and phase behavior of the cryo-mineral mirabilite that forms when the water column is cold may also play an important control on water density and the saturation state of halite. Furthermore, the shallow, low-gradient nearshore and mudflat environments behave similarly in response to seasonal changes and groundwater contribution as that of a saline playa system. Kirby and others (2019) surveyed the groundwater around GSL and recorded a range in concentration of dissolved solids. However, those concentrations, while elevated in many areas, are less than that of the north arm brine and undersaturated with respect to halite. If groundwater is discharging into the lake in the north arm, areas of discharge should be observable because the halite crust, if present, will exhibit dissolution textures. On a small scale, Rupke and others (2016) observed zones of halite dissolution pipes and smoothed crust surfaces in the nearshore halite crust, particularly after rain events. Dissolution of the halite crust by fresher groundwater input may recycle the dissolved solids and concentrate them at the lake center, which adds additional complexity to understanding the interaction between shallow concentrated brines and less saline groundwater brines.

Because the north arm, at times, is thermally stratified, the brine may behave similarly to the Dead Sea where seasonal thermohaline stratification produces depth-controlled variations of halite saturation and seasonal halite deposition in shallow and deep water (Arnon and others, 2016; Sirota and others, 2017). Several studies obtained detailed limnological measurements including monthly temperature and salinity profiles, degree of halite saturation, and the rate of halite precipitation in the water column, observed by underwater photography of the seasonal halite deposits (Arnon and others, 2016; Sirota and others, 2017). During winter, the water column of the Dead Sea is well mixed and the cooling of the bottom brine body results in rapid deposition of massive, fine-grained halite precipitates (cumulates). During summer, evaporation and heat influx create a saltier but warmer surface water layer (epilimnion) that subsequently becomes undersaturated with respect to halite due to higher temperature. Interestingly, dissolved salt in the warm and saltier epilimnion is delivered to the deeper, cooler brine (hypolimnion) by double diffusion, ultimately leading to halite supersaturation and accumulation along the lake floor (Sirota and others, 2017). The supersaturated lake floor is characterized by coarse, idiomorphic bottom growth halite crystals. In summary, the deep brine accumulates substantial amounts of finely crystalline halite during the winter and experiences slow growth of bottom halite crust during the summer. Although the chemistry and climate of the Dead Sea are different than GSL, we aim to test if the Dead Sea seasonal halite focusing model is like the deposition of halite in the north arm by adapting similar field and laboratory methods.

METHODS

To achieve our objectives of making systematic limno-sedimentological observations and field-laboratory geochemical measurements of the north arm salt system, we employed a variety of methods. These methods included underwater photography, measurement of halite precipitation rate and conditions of the north arm water column, documentation of nearshore precipitation of halite crust, and laboratory experiments on the state of halite saturation. Details of these various approaches are described below.

Field Observations and Brine Measurements

Field observations of the Spiral Jetty shoreline and ooid flat were made during late 2019, throughout the seasons of 2020, and the first half of 2021. Salt crust characteristics, thickness, and accumulation and the presence of groundwater discharge were noted. We also noted if salt rafts were forming on the north arm water surface. On some trips to the Spiral Jetty, we measured the nearshore salt crust thickness using the methods described in Rupke and others (2016). Samples of lake brine and groundwater spring seeps were collected and measured for major ion composition (Na^+, K^+, Ca^{+2}, Mg^{+2}, Cl^-, SO_4^{-2}, HCO_3^-), density, pH, temperature, and the analyses of

the stable water isotopes (δD and $\delta^{18}O$). Groundwater samples were collected directly from discharge zones and from a transect of six shallow (~ 3 ft deep) piezometers installed from east to west (lake margin towards the lake). The piezometers were installed by manual augering and secured with bentonite and silica sand. Major ions were measured with ion chromatography (IC) and inductively coupled plasma–atomic emission spectrometry (ICP-AES) at the American West Analytical Laboratories. Stable isotope analyses were performed by the Stable Isotope Ratio Facility for Environmental Research (SIRFER) laboratory at the University of Utah using a Picarro L2130i analyzer with cavity ring-down spectroscopy (CRDS). Stable isotope ratios (δ^2H_{VSMOW} $\delta^{18}O_{VSMOW}$) were normalized to the VSMOW/SLAP scale with two primary references and one secondary reference. Mineral identification for sediments that precipitated near spring discharge zones and within the lake was conducted with X-ray diffraction (XRD) using a Rigaku MiniFlex 2 detector and the software Match!* version 3.1 was used for processing the data.

Underwater Photography

In an effort to understand the precipitation or dissolution state of the salt crust and to potentially observe signs of groundwater upwelling, we deployed an underwater video camera from an inflatable boat or the Utah Division of Wildlife Resources (DWR) GSL Ecosystem Program boat in August, September, and October of 2019; June and September of 2020; and May of 2021 in multiple locations in the north arm: near the Spiral Jetty (shallow, ~10 ft), along the causeway (~25 ft water depth, representing the depocenter), and at brine sample sites LVG4 (~20 ft) and RD2 (~15 ft) (figure 1). To make these observations, we developed a versatile custom mount that allows a variety of camera and lighting positions for optimizing observations under varying conditions. The mount consists of a cubic steel frame (1 ft^3) that was lowered to the north arm lake floor using a nylon rope with locking carabiners. For photography we used a GoPro Hero 7(R) camera in a submersible housing equipped with a PolarPro SwitchBlade(R) macro lens and two LED dive lights (figure 6). Multiple attempts were required to determine the best camera and lighting positions and to achieve usable photography. The best positioning for the camera was typically pointing straight down a few inches (~3″) from the bottom floor. The best lighting was achieved by positioning the light sources at an angle to the area of focus to create textural contrast, and within a few inches of the surface. This provided the best imagery despite the high turbidity conditions in the water column that increase with depth (discussed below). Each video recording was evaluated for sedimentological characteristics of the north arm substrate and other environmental features. Individual video frames were captured and digitally sharpened to improve image quality.

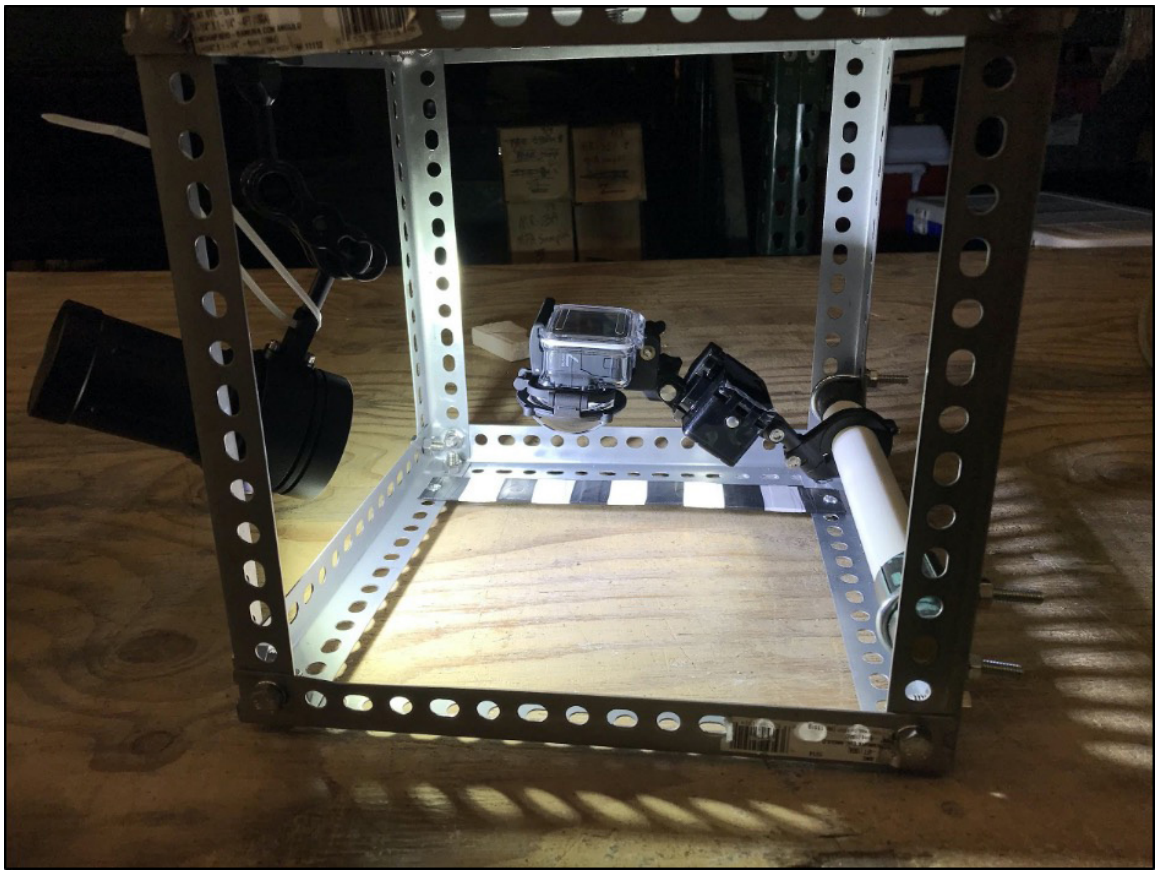

Figure 6. *Custom-made camera mount cage with white LED light sources. The camera is a GoPro Hero 7 in a submersible housing equipped with a PolarPro SwitchBlade(R) macro lens. White and black scale bar mounted to the frame is in 1-inch increments.*

Buoy Systems and Rate of Halite Precipitation

We attempted to measure the rate of halite precipitation in the water column by using methods developed by researchers who study the Dead Sea (Sirota and others, 2017). This measurement was done using a vertical rope tensioned by a buoy and anchor that periodically was checked for halite growth. If crystallization occurred, the depth intervals where halite precipitated along the water column were recorded and the diameter of the cylindrical coating of crystals around the line was measured with a caliper. In this study, a buoy attached by rope to a cinder block was used to keep rope tension. A secondary rope attached to the buoy was weighted with large steel washers and was intended to be used for measurements and observations. We deployed buoys at our photography sites near the causeway on August 1, 2019, and the Spiral Jetty on August 14, 2019, and September 2, 2020 (figure 1). The sites of investigation were chosen to record the macroscopic rate of halite growth within the upper epilimnion surface layer (Spiral Jetty) and deeper brine (causeway) hypolimnion. The buoy and line at the causeway were checked during September 2019, but were missing by June 2020 due to storm and wave activity. Similarly, the buoy and line offshore from the Spiral Jetty were checked in October 2019, but were absent by June 2020 due to storm events. A buoy deployed in September 2020 was located and examined in May 2021.

Water Profile Measurements

During September 2019 and May 2021, we deployed the UGS's Hydrolab MS5 mini sonde to collect water profile information including water depth, temperature, and turbidity. The instrument was calibrated at OTT Hydromet laboratories in Loveland, Colorado.

Density Experiments

In November 2019, multiple lake brine samples were collected in 50 mL sample bottles and the lake temperature was recorded. One sample from each duplicate represented a "control" and the other a 'test' or "spiked" sample filled with 10 g of NaCl. In the laboratory, the brine samples were kept at a variety of temperatures (including one set at lake temperature). To ensure that solids (salts) were in solution and in equilibrium with the brines, the experiments were performed for five days and agitated occasionally. Afterwards, the densities of the brines were measured with a portable Anton Paar DMA density meter (error of ±0.001 g/cm^3) and the difference between the values was used to determine the empirical degree of halite saturation (EHS). The EHS was recorded in sigma units (σkg/m^3) which is calculated by subtracting the reference density of pure water at the same temperature. A rise in density of the spiked brine with respect to the density of the control brine would indicate the sample is "undersaturated" with respect to halite, and, alternatively, a decrease in density (or, in some cases, a negligible differential) would indicate saturation. A simpler version of this experiment was repeated with samples collected on field visits during 2020 and 2021 in which a spiked sample and control sample were measured and compared for density at room temperature (~20°C). In addition, a handheld refractometer was used to measure the change in salinity of halite-saturated north arm brine at room temperature and after cooling to 0°C.

Geochemical Modeling and Halite Saturation States

Geochemical modeling of lake brine was performed from brine sampled at the Spiral Jetty on November 16, 2019. The sample was part of a round robin sampling campaign for the comparison of laboratory measurements by the GSL Salinity Advisory Committee (Great Salt Lake Salinity Advisory Committee, 2020). The modeling was focused on identifying mineral saturation states along evaporation pathways and at different temperatures. The same was done for groundwater seeps from the Spiral Jetty and Locomotive Springs from the northern part of the lake. The computer program PHRQPITZ was selected because it utilizes the Pitzer virial-coefficient model to calculate activity-coefficients and mineral saturation states for high ionic strength brines at various temperatures (Plummer and others, 1988), making it a suitable chemical modeling program for modeling north arm brine evolution.

RESULTS AND DISCUSSION

Nearshore Salt Crust and Groundwater Field Observations

During field visits to the causeway and the Spiral Jetty, we observed no substantive salt crust formation along the nearshore environment during the second half of 2019 or the first half of 2020 with the exception of ponded areas adjacent to the shore and isolated from the main body of the lake (figure 7). During the dry season of August to October, 2019, a thin (~1 inch thick) exposed, reworked, and wave-rippled halite crust was present at the lake water margins near the Spiral Jetty (figure 7A), but the crust did not extend into the lake waters (figure 7B). By June and July 2020, no halite crust was present along the shallow lake floor, and the thin, discontinuous shoreline halite crust had dissolved (figure 8). However, by mid-August 2020, a coarsely crystalline crust formed on the floor below the water surface and by early September that crust was fully pervasive below the water surface along the nearshore. In tandem with salt crust formation, we observed salt rafts forming on the lake water surface by mid-August 2020. Additional observations are recorded in appendix A. By late October 2020, a substantial nearshore crust had formed and we measured salt crust up to 3 inches thick along our transect where crust was absent in the prior season (and likely for the last few years) (figures 9 and 10, appendix B). Between December 2020 and early May 2021, the submerged nearshore salt crust dissolved

away entirely (figure 10, appendix B). However, on May 25, 2021, we observed salt rafts forming on the water surface at sites RD2 and near the Spiral Jetty (on the same day we did not observe rafts at LVG4) and in early June 2021 at the Spiral Jetty a patchy nearshore salt crust was present in shallow water, salt rafts were forming on the brine surface, and broken halite rafts formed several small beach bars along the shore due to wave action. A salt crust was absent in water deeper than a few inches. Figure 11 shows density measurements of brine samples collected during our field visits as well as our interpretation of halite saturation state based on field observations of north arm conditions (thickness of salt crust, presence of salt rafts, etc.). We did not consider the north arm to be saturated when only limited halite was present along the shoreline or in slightly restricted shallows and ponds; in general, we considered the north arm to be supersaturated when rafts were forming in the main body of the lake (as opposed to only in slightly restricted shallows) and/or crust was forming in water depths of more than a few inches. We also took our crust thickness measurements into account. Based on these measurements and observations, halite saturation in the north arm appears to occur at a brine density of about 1.222 g/cm^3 or slightly higher (at 20°C) (figure 11).

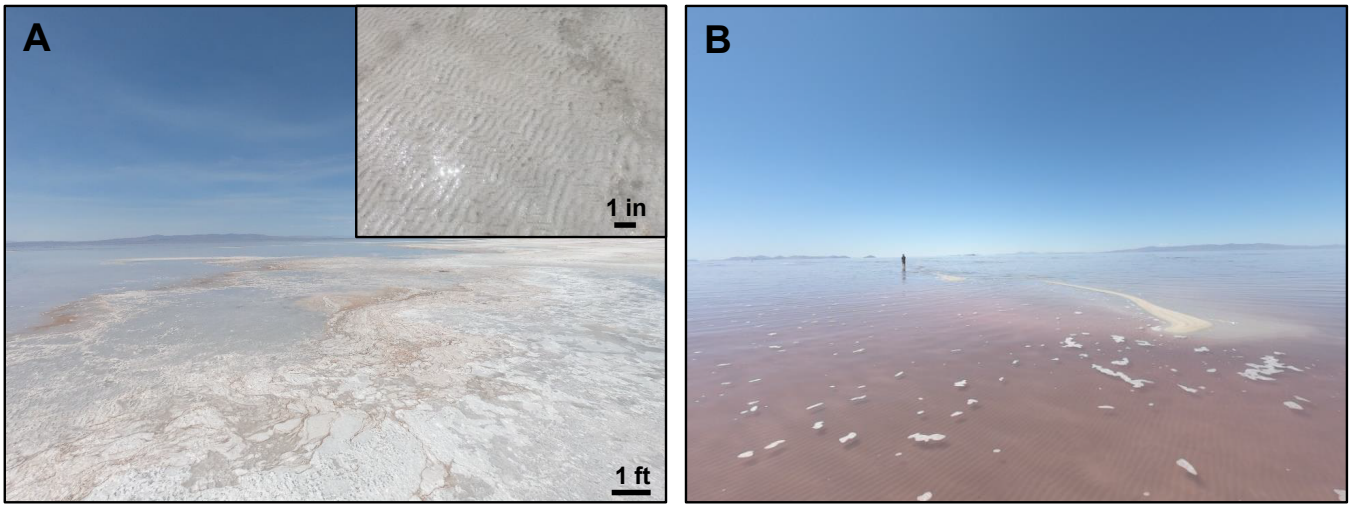

Figure 7. *Dissolved and reworked halite crust observed near Spiral Jetty in October 2019.* ***A)*** *Reworked thin halite crust (0.8 inches thick) observed near the lake shore with subtle ponding of brine. Inset shows asymmetric interference ripples composed of rounded halite hopper grains. View is to the northwest.* ***B)*** *View looking west, about 10 ft from the halite encrusted shore. Note the absence of subaqueous halite accumulation and halite rafts (floating white objects are foam). Ooid sand bar and asymmetric ripples imply wind and storm events alter the shoreline. Person for scale.*

Figure 8. *The shoreline near Spiral Jetty in June 2020. A halite crust is absent and only ooid sand is exposed. The white is foam and the blocky rocks are ancient (Bonneville age?) carbonate microbialite deposits. View is to the southwest. Shovel for scale.*

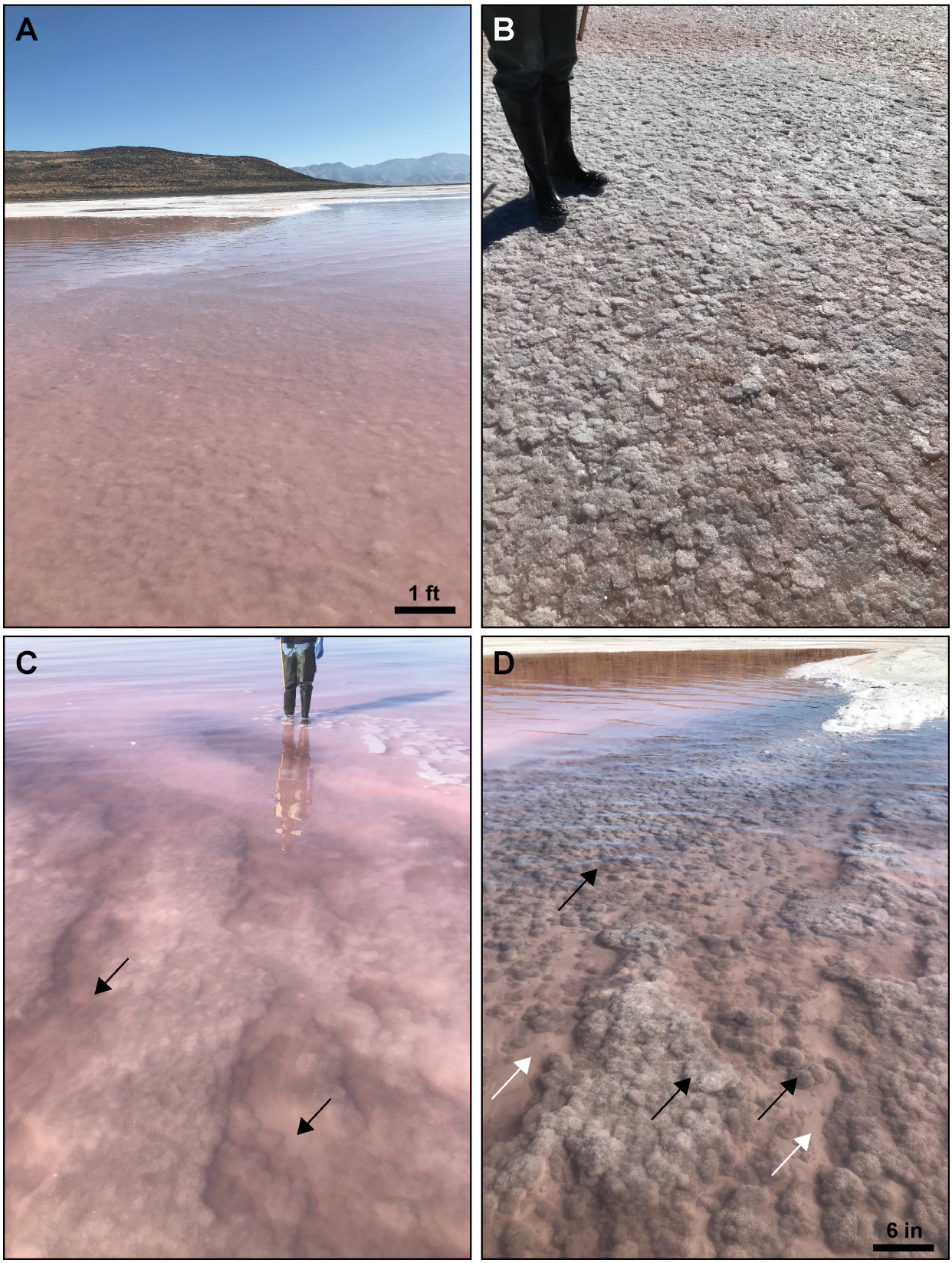

Figure 9. *Halite crust along the shoreline near Spiral Jetty during late October 2020.* ***A)*** *Submerged halite crust composed of bottom growth chevron crystals and aggregated halite rafts. View is to the east.* ***B)*** *Collection of exposed halite rafts that accumulated in a ponded depression inland from the shoreline.* ***C)*** *and* ***D)*** *Subaqueous linear, patchy relief, and isolated rounded halite bottom crust along ooid-mud beach bars (black arrows). Note sediment fill between halite clusters (white arrows). Halite crystals appeared partially smooth and the patchy fabric suggests the shallower water depth along the beach bars promotes mechanical reworking by waves and/or the beach bars act as groundwater upwelling zones.*

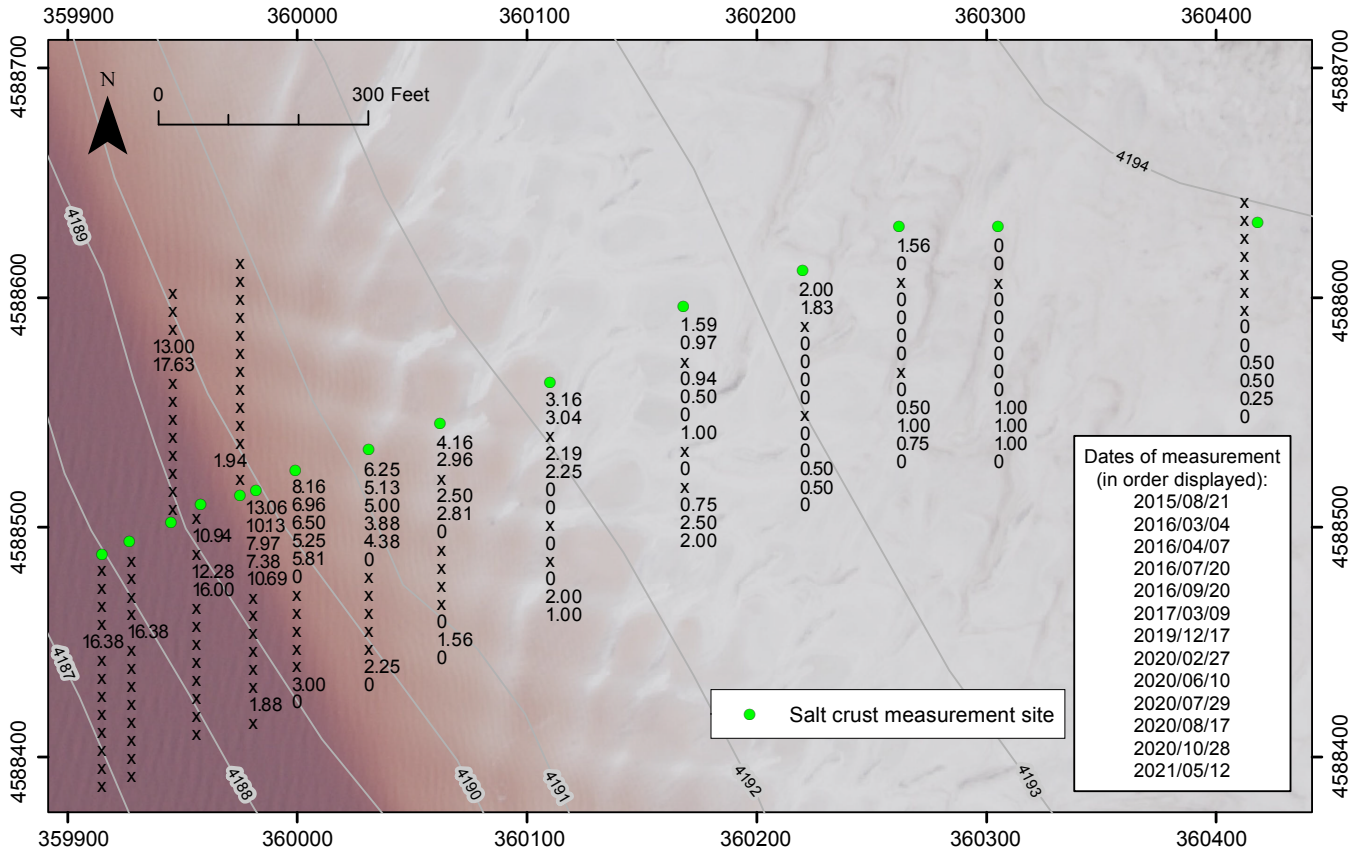

Figure 10. *Nearshore salt crust thickness measurements from near Spiral Jetty. Thicknesses are in inches. An "x" indicates that a measurement was not taken (typically because it was inaccessible) at the site on that date. Aerial photography is 2018 NAIP provided by the Utah Geospatial Resource Center. Topographic contours are in feet and are from Baskin and Turner (2006). Coordinates are UTM Z12 NAD83 meters.*

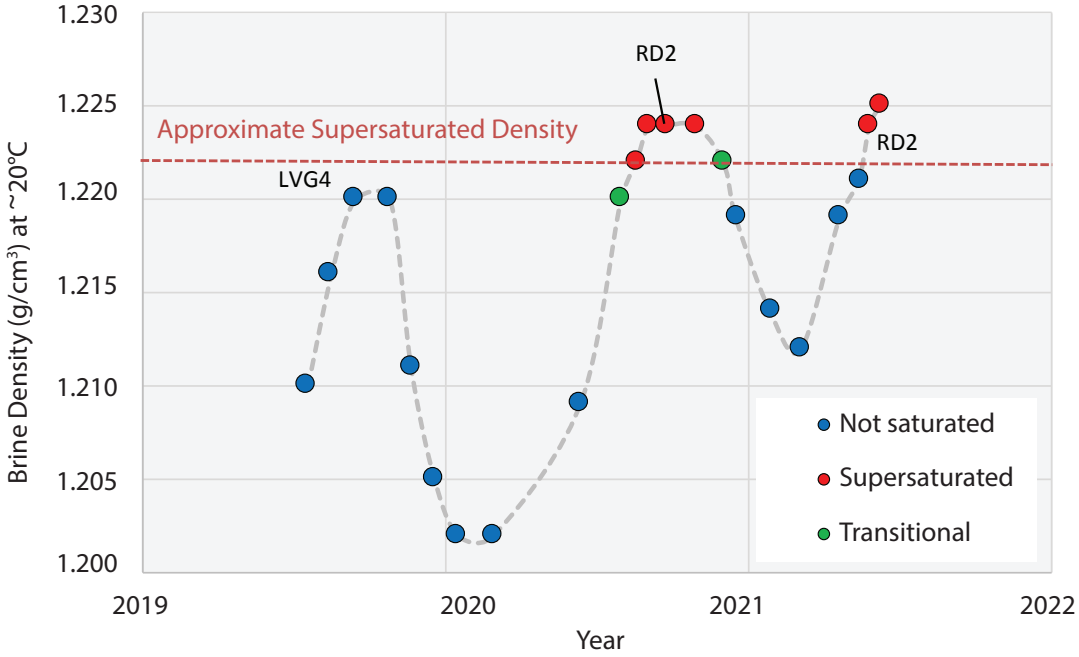

Figure 11. *Density measurements and inferred halite saturation state of the north arm brine based on field observations during the study period. Density measurements are from Spiral Jetty with the exception of labeled points. Saturation state for this graph was determined from field observations such as a nearshore submerged salt crust, measured salt crust thickness, or salt rafts on the water surface. Observations for points designated as "transitional" were deemed ambiguous. The saturation state of multiple points in early 2021 is inferred from the measured salt crust loss between October 2020 and early May 2021 (appendix B). All density measurements from late 2020 through 2021 were at 20°C and measurements prior to that were from 21°C to 23°C. Field observations are recorded in appendix A.*

In summary, nearshore observations indicate that negligible halite precipitation occurred during 2019 and through the first half of 2020. The north arm then reached supersaturation in early August 2020 and remained supersaturated through late October 2020. By mid-December the north arm became undersaturated until mid-May 2021. In mid-May 2021 the north arm again reached supersaturation. Although we have limited observations from 2018, we consider it likely that significant halite precipitation did not occur in the north arm until late 2020 following the opening of the new causeway bridge in December 2016. Although saturation was reached in summer 2020 and late May 2021, measured densities of the north arm brine recorded during this study did not approach the high densities recorded in late 2016 prior to the opening of the causeway bridge (up to 1.232 g/cm^3 at ~22°C) (Utah Geological Survey, 2020).

As with most winter seasons in the north arm, during the winters of 2018-19, 2019-20, and 2020-21, the shoreline and nearshore lake waters precipitated and accumulated a hydrated mirabilite mush (figure 12). Storm events and lake currents formed mirabilite beach bars up to 2 ft thick (figure 12A). It is likely that mirabilite not only precipitated in nearshore environments but also in the deeper parts of the north arm. During the warmer seasons mirabilite is absent in the nearshore environment because it dehydrates to thenardite (Na_2SO_4), a white chemical powder that eventually dissolves or speciates into Na^{2+} and SO_4^{2-} in the warmer waters.

Groundwater spring seeps with lower salinities than lake waters (densities of ~1.072 g/cm^3) were also noted along the shoreline and lake margin during October 2019 through March 2021. The springs had a pH range of 5.6 to 7.1 (tables 1 and 2). Seeps near the lake shore and on the ooid flat are circular shaped depressions that vary in diameter from 0.5 to 2.0 ft. They have the appearance of mini-sinkholes and are interpreted as areas of sediment collapse where the underlying porous ooids allow groundwater to flow upward and cause the surface sediment to collapse on itself. Most of the seep holes were ~3 ft deep and some were as much as 6 ft deep. Because the hydraulic head spatially changes on the ooid flat and nearshore environment, the seep holes often dry out, fill with sediment, or become clogged with halite or mirabilite during winter months. During October 2019, less saline groundwater emerged in a seep hole nearshore and partially dissolved the halite crust (figure 13A). In late October 2020, when there was a substantial nearshore crust, we observed linear and patchy halite crusts within shallow water along the tips of ooid beach bars on a calm weather day (figure 9C, D). The patchy halite crusts trended perpendicular to the shore and displayed a rounded, puffy texture. Sediment between the crusts was mainly peloidal mud with ooids and below the sediment the brine temperature was lower than lake water. This suggests some form of upwelling of less saline groundwater in the nearshore environment may be occurring. In addition, in June 2021 we witnessed mechanical reworking of the patchy halite crusts by wave

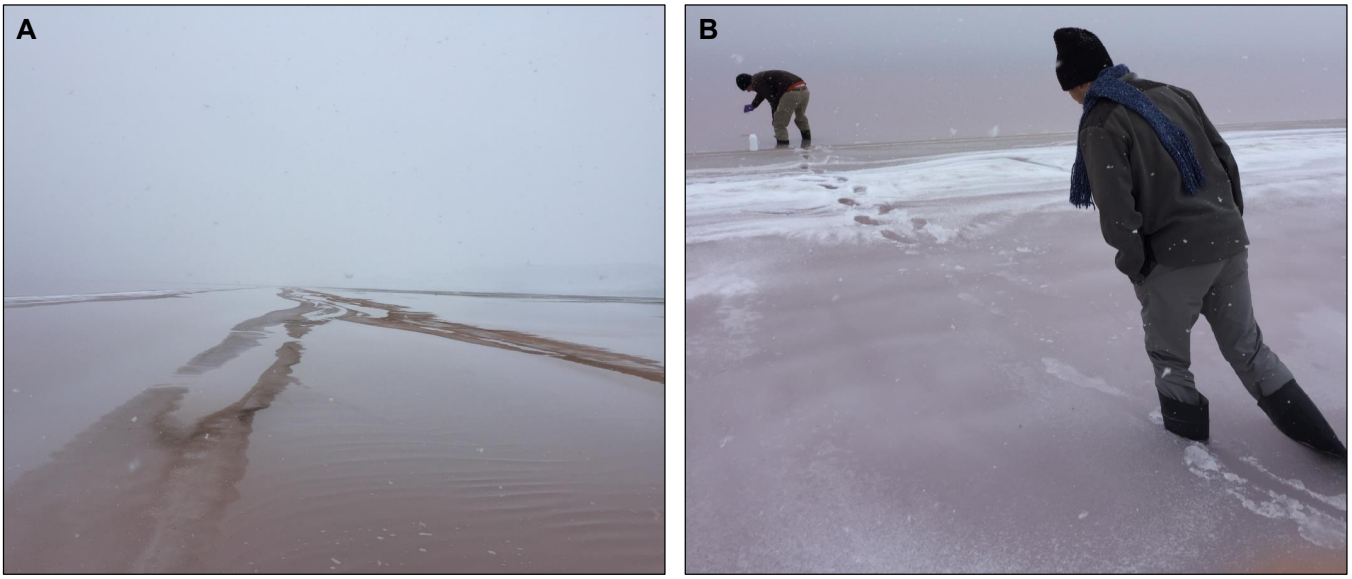

Figure 12. *Spiral Jetty area in January 2019 showing accumulation of mirabilite.* ***A)*** *Beach bars of mirabilite 3 ft wide in 1 ft of lake brine.* ***B)*** *Photograph showcasing the texture of mirabilite as a chemical mush around 2 ft thick.*

Table 1. *Temperature, density, pH, and general observations at field sites for the precipitation of halite. Densities were measured at room temperature (~22°C).*

Site	Date	Depth (ft)	Lake T °C	Density (g/cm^3)	pH	Observations
Spring seep #1 SJ-1	October 4, 2019	0.2	14.4	Not measured	7.1	efflorescent halite
Spring SJ4	October 4, 2019	near surface	10.0	1.072	6.6	halite dissolution
Spring seep #3 SJ-1	October 5, 2019	near surface	15.0	1.065	5.6	halite dissolution

Table 2. *Chemistry of groundwater and springs adjacent to Great Salt Lake's north arm. Samples SJ1 through SJ4 and SJP1 through SJP6 were collected during this study. Additional chemistry is from Kirby and others (2019) from around Spring Bay.*

Site	Easting UTM	Northing UTM	Date Sampled	Location	Temp. (°C)	pH	Na^{+} (g/L)	Mg^{+2} (g/L)	K^{+} (g/L)	Ca^{+2} (g/L)	Cl^{-} (g/L)	SO_4^{-2} (g/L)	HCO_3^{-} (g/L)	TDS (g/L)	δ^2H_{VSMOW}* (‰)	$\delta^{18}O_{VSMOW}$ (‰)
SJ1	360615	4588727	8/17/2020	North Arm lake	23.1	7.1	114	13	7.94	0.34	200	26.7	0.30	300	-67.3	-3.7
SJ2	360846	4588606	3/03/2021	Spiral Jetty	_	7.0	39.9	2.23	1.65	0.87	70.6	5.79	0.2	114	-84.6	-6.8
SJ3	360786	4588649	3/03/2021	Spiral Jetty	5.4	7	22.8	1.37	1.26	0.37	40.3	4.46	0.56	68.9	-90.3	-8.9
SJ4	360583	4589075	3/03/2021	Spiral Jetty	9.7	7.1	31.8	1.81	1.45	1.19	55.9	8.09	0.16	32.6	-91.2	-7.8
SJP1	360584	4589074	3/24/2021	Spiral Jetty	9.6	7.3	75.4	4.39	3.02	0.7	126	19.2	0.15	20.7	-74.6	-4.6
SJP2	360558	4589062	3/24/2021	Spiral Jetty	10.6	6.9	61.7	3.93	2.73	0.63	109	23.8	0.25	158	-77.8	-6.3
SJP4	360552	4589058	3/24/2021	Spiral Jetty	8.7	7.2	88.4	7.26	4.67	0.37	167	30.2	0.35	268	-72.0	-3.9
SJP5	360256	4588801	3/24/2021	Spiral Jetty	10.7	7.0	107	9.95	5.98	0.23	198	37.8	0.45	304	-67.3	-3.8
SJP6	360065	4588643	3/24/2021	Spiral Jetty	10.9	7.3	105	10.3	6.34	0.26	203	34.3	0.37	294	-70.3	-4.4
West spring	323180	4608090	12/30/2015	Spring Bay	_	7.8	2	0.102	0.078	0.138	3.480	0.208	0.234	6.059	-126.0	-16.2
West spring2	320787	4617548	11/15/2017	Spring Bay	12.4	7.4	2.769	0.071	0.140	0.209	5.398	0.118	0.208	8.913	-128.4	-16.9
West spring3	321333	4618990	11/14/2017	Spring Bay	12.2	7.0	nd	nd	nd	nd	nd	nd	nd	nd	-115.1	-15.7
East Spring Bay	354524	4611108	11/16/2017	Spring Bay	14.4	5.0	5.264	0.229	0.268	0.177	9.308	0.782	0.285	16.313	-113.8	-14.3
Locomotive spring	340143	4619353	8/29/2005	Spring Bay	15.9	7.2	0.580	0.062	0.041	0.142	1.095	0.112	0.247	2.166	-132.2	-17.0
SaltWell Rd	355886	4622255	11/15/2017	Spring Bay	18.3	7.4	3.055	0.098	0.140	0.243	5.386	0.158	0.251	9.331	-126.3	-16.2

*Stable isotopes were normalized to the Vienna Standard Mean Ocean Water (VSMOW) isotopic standard scale.

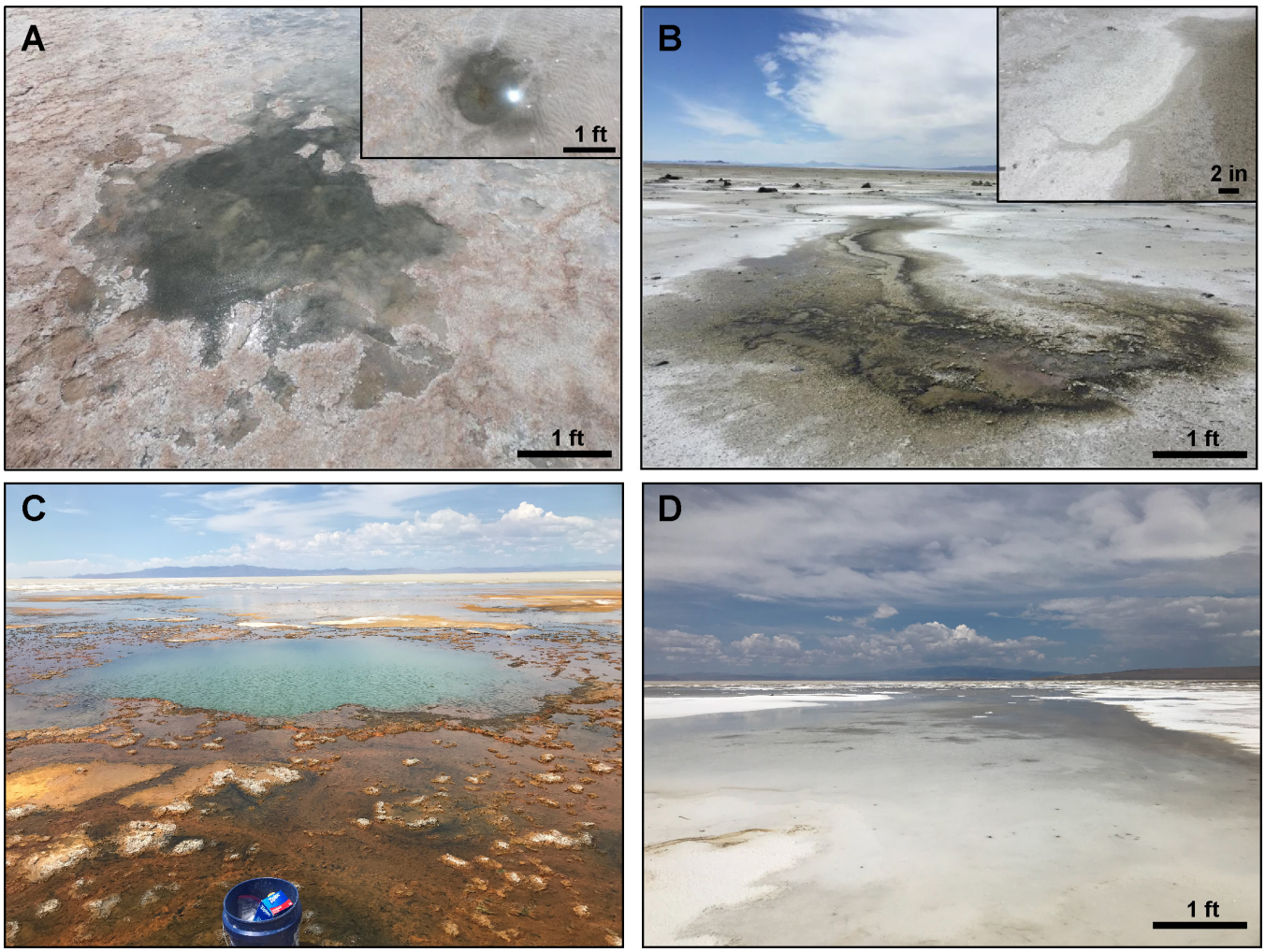

Figure 13. *Spring seeps near Spiral Jetty in October 2019 (A and B) and exposed lake spring near Spring Bay in June 2021 (C and D).* ***A)*** *Spring seep #3, about 3 ft deep, that partially dissolved the surrounding halite crust. Inset shows a spherical sediment collapse spring seep (1 ft wide) nearby, implying areas of porous ooid sands where upward-directed groundwater flow collapsed below the halite crust sediment.* ***B)*** *Marginal spring seep SJ4 discharging into desiccated mudflat polygons. The groundwater had a density of 1.072 g/cm^3, pH of 6.6, and precipitated carbonate near the seep (see figure 15 for X-ray diffraction plot and figure 33 for mineral saturation). Brine flies were also present in the spring pool, confirming less saline groundwater. The spring waters drain into polygonal depressions (inset photograph) where gypsum selenite crystals precipitate, and later, a veneer of halite epifluorescent crust forms.* ***C)*** *Large spring hole near Spring Bay actively discharging saline groundwaters. The spring pool is 22 ft wide and ~ 12 ft deep with a laboratory-measured density of 1.046 g/cm^3 at 20°C and field-measured salinity of 8% at 22°C. Carbonate crusts and microbialites form near and around the discharge zone and construct mini-rimstone dams and pools from low-gradient flow.* ***D)*** *The saline groundwaters discharge away from the spring hole shown in (C) into topographic low areas, evaporate, and precipitate halite as a 1-inch-thick crust. Wind blows and ponds the spring waters over an area of ~ 1.2 mi^2.*

action on a windy day and the mud was gone and replaced by ooid sand. This highlights the dynamic processes that occur at the nearshore environment.

Lake margin spring seeps were also observed that discharged into desiccated polygonal mudcrack depressions (figures 13B and 14). Evaporation and concentration of the less saline brine initially precipitated carbonate (calcite/aragonite) and gypsum, confirmed by hydrochloric acid and XRD (figure 15), followed by a thin halite efflorescent crust (figure 13B). This observation is significant because after a storm surge or seiche, the spring seep solutes and thin halite crust may be recycled back into the lake, as indicated by drainage channels and bed forms directed towards the lake. To test if lake margin groundwaters evolve to north arm lake brine or mix with mudflat groundwaters, 6 piezometers were installed that transected away from the main discharge zone of spring SJ4 (see Geochemistry section for related discussion) (figure 14). In June 2021, a large prismatic spring hole was discovered near Spring Bay (figure 13C). The spring circumference is 22 ft wide with an approximate depth of 12 ft that was actively discharging saline groundwater that had a laboratory-measured density of 1.046 g/cm^3 at 20°C and a field-measured salinity of 8% at 22°C. The walls of the spring hole are lined with carbonate cement and subaerial rimstone dams and pools surround the perimeter formed by low gradient flow and the precipitation of carbonate (figure 13C). Interestingly, modern subaqueous microbialites actively grow along the walls of the spring hole at a depth of ~1 ft, well within the photic

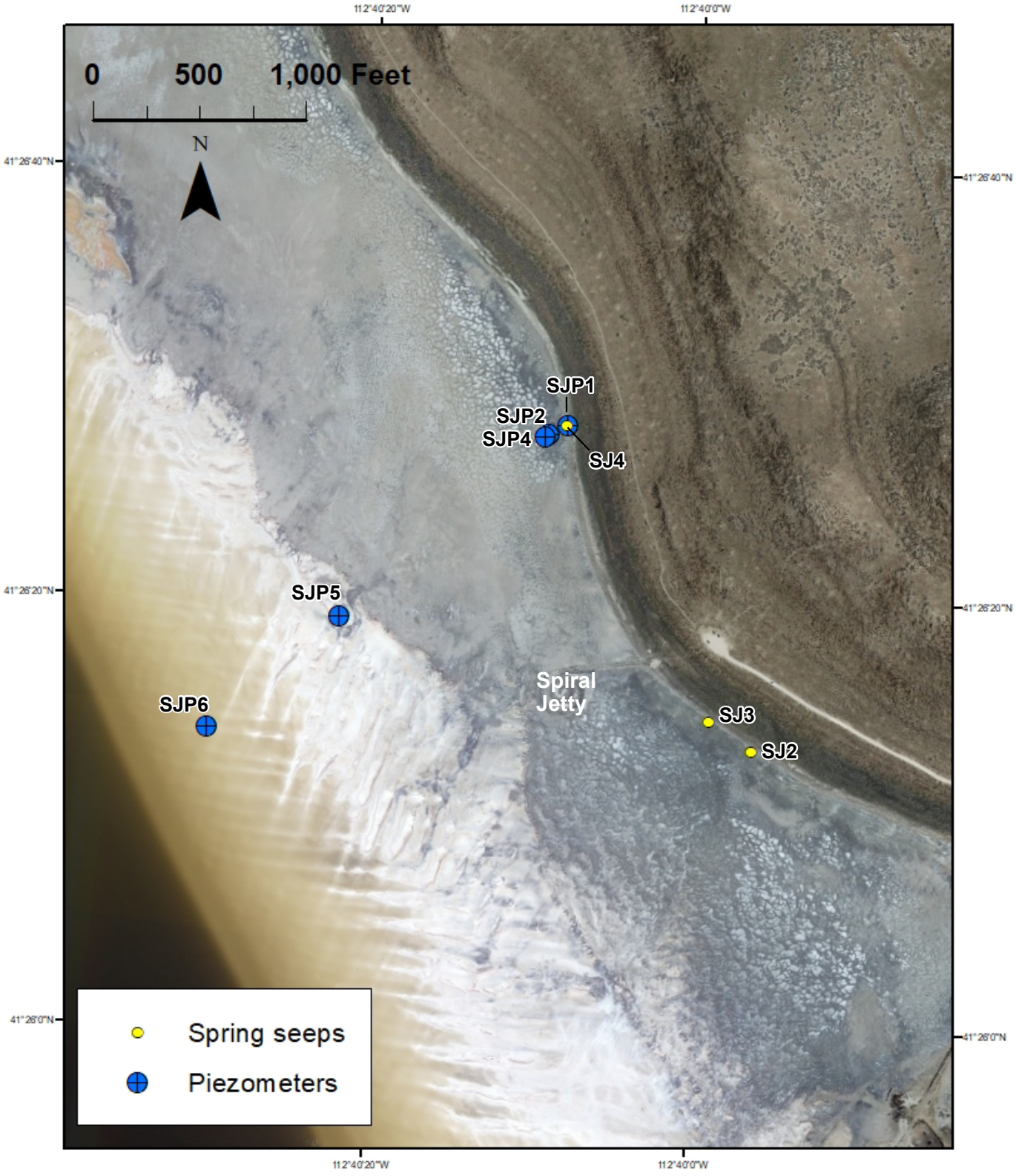

Figure 14. *Spring seep and piezometer locations at Spiral Jetty. Satellite Google imagery is from 2014 when lake elevation was higher (~4193 ft) and does not depict current lower lake level.*

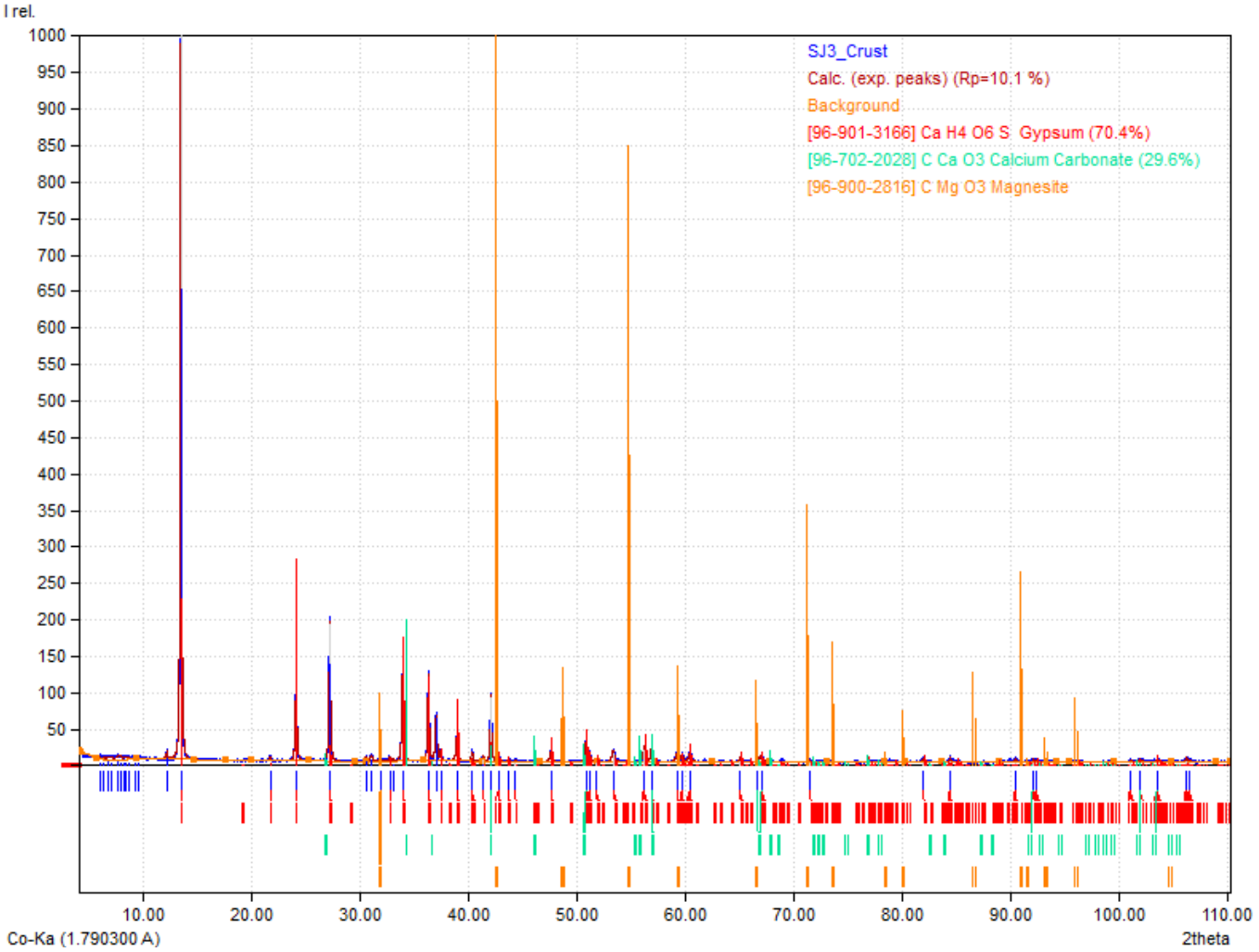

Figure 15. *X-ray diffraction pattern of precipitated chemical crust from marginal spring seep SJ4, sample ID SJ3_Crust (blue) (figures 7D and 13). X-axis is degrees 2theta (the angle of between transmitted and reflected beams) and the y-axis is relative peak intensity. The high intensity peaks are gypsum (red) that overlap with calcite/aragonite peaks (green). Subordinate peaks are an unknown carbonate (protodolomite, magnesite?) (orange; i.e., magnesite) and probable clay minerals from the crust forming on the oolitic-clay bound mudflat. "Calc. (exp. peaks)" refers to an unknown reference pattern.*

zone. The discharge waters drain away from the source point several hundreds of feet into topographic lows and are also pushed by wind. Over time, evaporation of the saline groundwater can precipitate an efflorescence halite crust covering an area >1.2 mi^2 on the exposed lake bed surface (i.e., mudflat).

Underwater Photography

We captured underwater imagery near the causeway on August 1, 2019, September 4, 2019, June 3, 2020, and September 28, 2020; near the Spiral Jetty on August 14, 2019, October 24, 2019, September 2, 2020, September 23, 2020, and May 25, 2021; at LVG4 on September 23, 2020, and May 25, 2021; and RD2 on September 23, 2020, and May 25, 2021 (figure 1, table 3). Initially the camera and lights were not well positioned and the imagery from August 1, 2019, did not yield clear/interpretable results. However, subsequent setups yielded results allowing us to infer, to some degree, the state of the salt crust. On August 14, 2019, near the Spiral Jetty at a water depth of about 10 ft, we observed an unobstructed view of the lake floor showing a relatively smooth, hard, planar surface of interlocking halite crystals (figure 16). Although the surface was primarily smooth, a white residue was present in areas and along some crystal interfaces, as well as particles floating within the water column. Shortly thereafter, on September 4, 2019, images collected near the causeway at a depth of about 25 ft showed a white, very fine grained, unconsolidated layer of sediment on the lake floor salt crust, although in one image some of the crystalline halite substrate appeared to be visible (figure 17). The white sediment layer is thin, likely a fraction of an inch (perhaps about 0.08 to 0.25 inches thick), based on the scale bar and how the camera mount was positioned. On October 24, 2019, we captured images offshore from the Spiral Jetty at a depth of about 10 ft showing a similar white sediment layer, but the sediment was wave-rippled and a hint of a crystalline halite substrate appeared to be visible (figure 18). Upon returning to the causeway on June 3, 2020, at a water depth of about 25 ft, we again observed a thin, featureless sediment layer (figure 19). At times when the camera cage was dragged

Table 3. *Summary of findings from underwater photography in relation to the saturation state of the lake floor.*

Photography Date	Description	Interpreted Saturation State
August 1, 2019	Poor images	not determined
August 14, 2019	Spiral Jetty, smooth and dissolved crust surface	undersaturated
September 4, 2019	Causeway, smooth crust covered with white sediment	undersaturated
October 24, 2019	Spiral Jetty, smooth crust covered with wave-rippled white sediment	undersaturated
June 3, 2020	Causeway, smooth crust covered with white sediment	undersaturated
September 2, 2020	Spiral Jetty, coarse-grained halite crystals and sunken salt rafts	supersaturated
September 23, 2020	LVG4-RD2-Spiral Jetty, coarse-grained halite crystals and sunken salt rafts	supersaturated
September 28, 2020	Causeway, coarse-grained halite crystals and sunken salt rafts	supersaturated
May 25, 2021	LVG4-RD2-Spiral Jetty, coarse-grained halite crystals	supersaturated

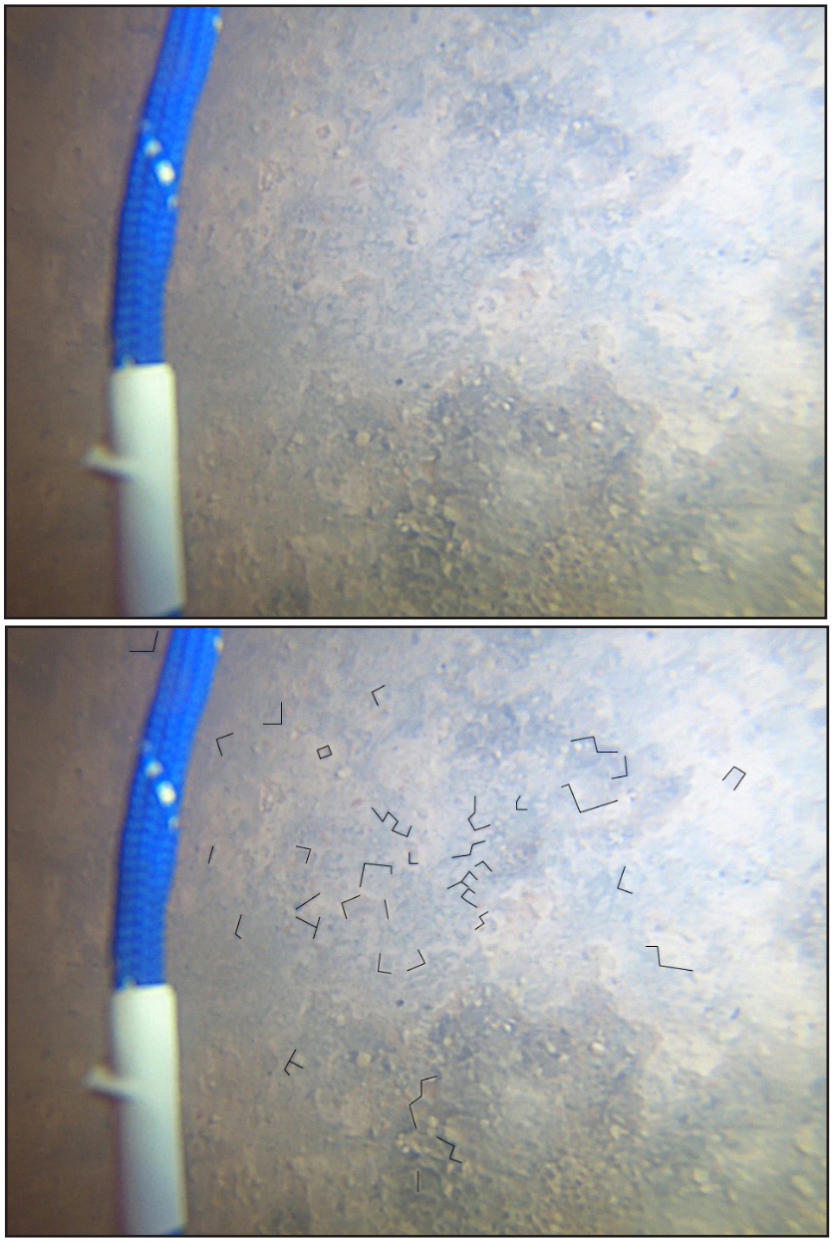

Figure 16. *North arm deeper basin salt crust showing crystal edges and interfaces. The smooth crust shows little or no relief, suggesting a surface that has been dissolved. This image was taken near the Spiral Jetty on August 14, 2019, in about 10 ft of water. The top photograph shows the original, sharpened image and crystal interfaces have been outlined in the bottom image. A light-colored residue of unknown composition seems to be present in areas and at times along crystal interfaces. The length of the white tape on the blue cord in the foreground is approximately 1 inch.*

Figure 17. *Thin, unconsolidated sediment layer covering the salt crust. The images were captured near the causeway at a water depth of about 25 ft on September 4, 2019. Scale on right is in inches. (Top) Lower left hand corner shows where camera mount scraped the unconsolidated sediment. (Bottom) Underlying halite crust appears to be visible near the center of the image. A few halite crystal interfaces may be visible in this area. Note crystal tops have minimal relief suggesting truncation by dissolution. Lake bottom appears to have an undulating wave-rippled surface.*

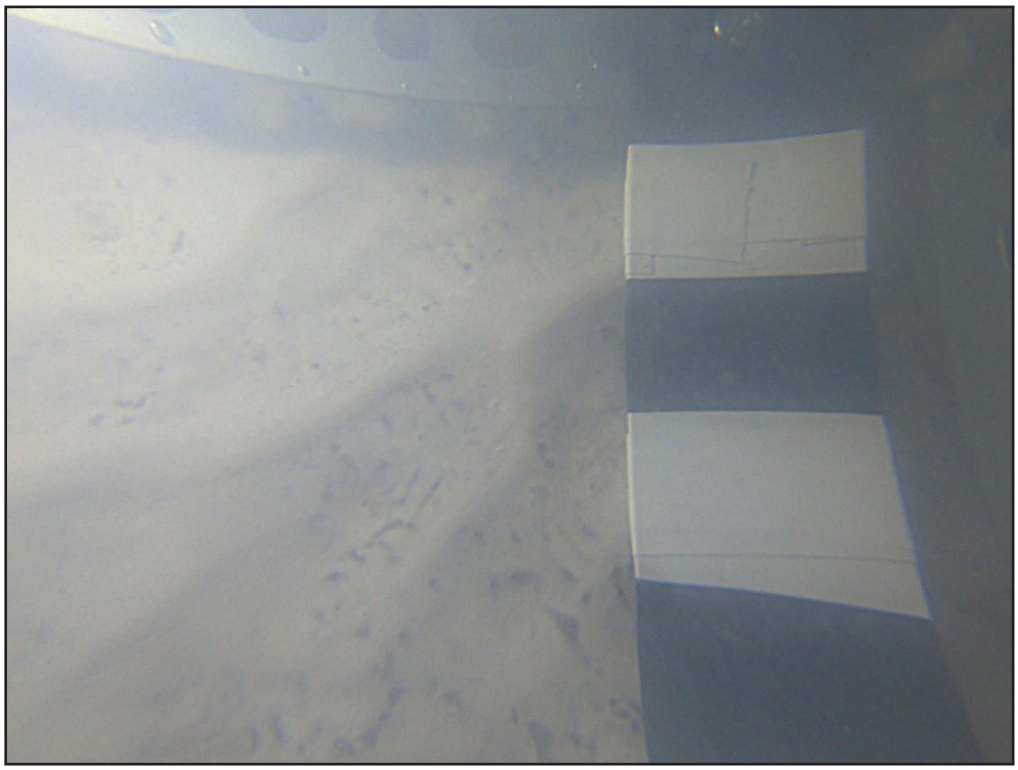

Figure 18. *Ripple-marked, white sediment layer on surface of salt crust. The thickness of the white sediment is estimated to be 0.12 to 0.25 inches and the crystalline halite substrate appears to be visible as dark patches and linear features (perhaps representing crystal interfaces). Note crystal tops have minimal relief suggesting truncation. This image was captured near the Spiral Jetty at a water depth of about 10 ft on October 24, 2019. The scale on the right is in inches.*

Figure 19. *Thin, featureless white sediment layer covering the salt crust. The salt crust's presence is inferred due to the hard, solid substrate encountered when lowering the camera mount. Image captured near the causeway at a water depth of about 25 ft on June 3, 2020. Scale on right is in inches.*

along the substrate due to boat drift, some filamentous textures (microbial mat?) were observed being ripped off the lake bottom. We consider it important to note that the camera mount always encountered a solid substrate, so we see no reason to doubt the presence of the solid salt crust even if obscured by the thin, unconsolidated sediment layer. In contrast, in the south arm, a soft, muddy substrate was always encountered. We also noted organic matter (and possibly mineral precipitates?) floating within the water column on all deployments, and, at times, a 1- to 2-mph current moving debris along the lake floor. The combination of the subtle undulated surfaces (possibly wave-ripples; figure 17) and a current implies the wave-base extends down to at least 25 ft.

In contrast to what we observed in 2019 and June 2020, photography from September 2020 showed a different substrate texture. Images captured at the Spiral Jetty, the causeway, site LVG4, and site RD2 during September 2020 all showed coarse, crystalline halite on the floor of the north arm (figure 20). The size of the halite crystals observed (~0.05 to 0.5 inches) is consistent with upward-directed crystal growth reported by Goodwin (1973), Woodhall (1980), and Rupke and others (2016). Some images also show finer-grained crystal clusters that overlie the coarser substrate and are likely to be sunken halite raft cumulates (figure 21). The presumed rafts are irregularly shaped and patchy, but dimensions range from about 0.5 to 2 inches wide. In some images we also saw a coating of a white, fine grained residue that drapes coarse crystalline boundaries or possibly as occluded impurities within the crystalline matrix (figure 22); we are uncertain of the significance or composition of the residue. In late May 2021, we again observed coarsely crystalline halite on the floor of the north arm that commonly had a white, chalky residue interstitial to the halite crystals (figure 22). Additional underwater images are presented in appendix C.

Our images of the north arm floor from 2019 and June 2020 suggest that the salt crust was undersaturated and in a state of dissolution at those times. In particular, images collected offshore from the Spiral Jetty (~10 ft water depth) on August 14, 2019, show a smooth, crystalline surface indicative of dissolution (figure 16). The image from figure 16 is similar to the subaerially exposed dissolved salt crust observed by Rupke and others (2016) (figure 23). However, the coarsely crystalline salt crust and submerged salt rafts observed in September 2020 are indicative of the north arm being supersaturated and actively precipitating salt crystals. Notably, halite growth on the north arm floor was occurring at all depths up to about 24 ft, where our deepest observations were made. These types of observations are consistent with what Rupke and others (2016) and Rupke and Boden (2020) observed during times of significant salt precipitation in 2015 and 2016 (figure 5). Goodwin (1973) also noted coarse crystals of halite (typically 0.08 to 0.16 inches, but up to about 0.4 inches) in salt crust core examined from deeper parts of the lake in the north arm. The significance of the coarsely crystalline halite that we observed in late May 2021 is less clear. Other observations (nearshore crust observations, density measurements, etc.) suggest that the north arm had only just reached saturation when we collected the images, and the coarse crystallinity may indicate very recent growth or that limited dissolution of the salt crust occurred in deeper water during the winter of 2020-21 (as opposed to dissolution of at least 3 inches that we measured in the nearshore environment). Our observations and interpretations of the photography are summarized in table 3.

Regarding the white sediment layer, as with our initial images from the Spiral Jetty in 2019, the remaining images from 2019 and June 2020 that show the unconsolidated sediment layer also indicate a smooth substrate. As our images from late 2020 suggest, if substantial crystal growth were occurring, it should be evident through the thin sediment layer. The significance of the white sediment is uncertain at this time. Preliminary XRD analysis conducted on the white sediment identified a predominant mixture of halite and a sulfate phase, probably mirabilite, although other phases may be present (figure 24). Because the sulfate mineral is hydrous, it is possible that during preparation on the XRD sample stage and scanning time the sediment dehydrated or changes in preferred crystalline orientation occurred, hindering peak intensity and position for interpretation. At this time more sediment sampling from the north arm substrate needs to be done to better understand the mineralogy of the white sediment and to determine if there is any associated organo-mineralic material present. A possible explanation for the sediment is that it represents a detrital (halite?) residual from dissolution of the salt crust or disintegrated mirabilite. During our underwater photography, we imaged significant turbidity in the water column and the sediment could be an accumulation of the material that makes up the turbidity (figure 25). Perhaps related, we also saw a milky turbidity in spring seeps that were forming mirabilite, suggesting that the turbidity could potentially represent evaporite crystallization. In addition, we placed 50 mL of a halite-saturated brine sample, collected on June 5, 2021, from the shore near the Spiral Jetty, in a freezer for one day at 0°C and clear bladed and tabular crystals of mirabilite formed (figure 25C). After several hours at room temperature (~23°C), the mirabilite crystals dissolved to a white, milky and finely crystalline mush (figure 25D).

During our final deployment of the camera on May 25, 2021, images collected at LVG4 showed some circular to irregularly shaped cavities (figure 26). Some of the circular cavities/holes (figure 26A) have a faint rim (figure 26B) or smoothing roundness (figure 26C) suggestive of halite dissolution and recrystallization. Although some of the dissolution zones appear to be small and isolated (figure 26A), we observed one linear zone of dissolution (figure 26D). These features bear some resemblance to dissolution zones and pipes photographed by Rupke and others (2016) near the water surface (see figure 5 of that publication). Therefore, we interpret these lake floor features to be dissolution pipes and zones of dissolution (and salt crust collapse?) by upwelling groundwater. The extent of these features is unknown, but we only observed them at LVG4 during a single expedition; however,

Figure 20. *Coarsely crystalline bottom growth halite crystals on the floor of the north arm. (Top) Image captured near the Spiral Jetty at a water depth of about 7 ft on September 2, 2020. (Bottom) Image captured at site RD2 at a water depth of about 16 ft on September 23, 2020. Scale on right is in inches.*

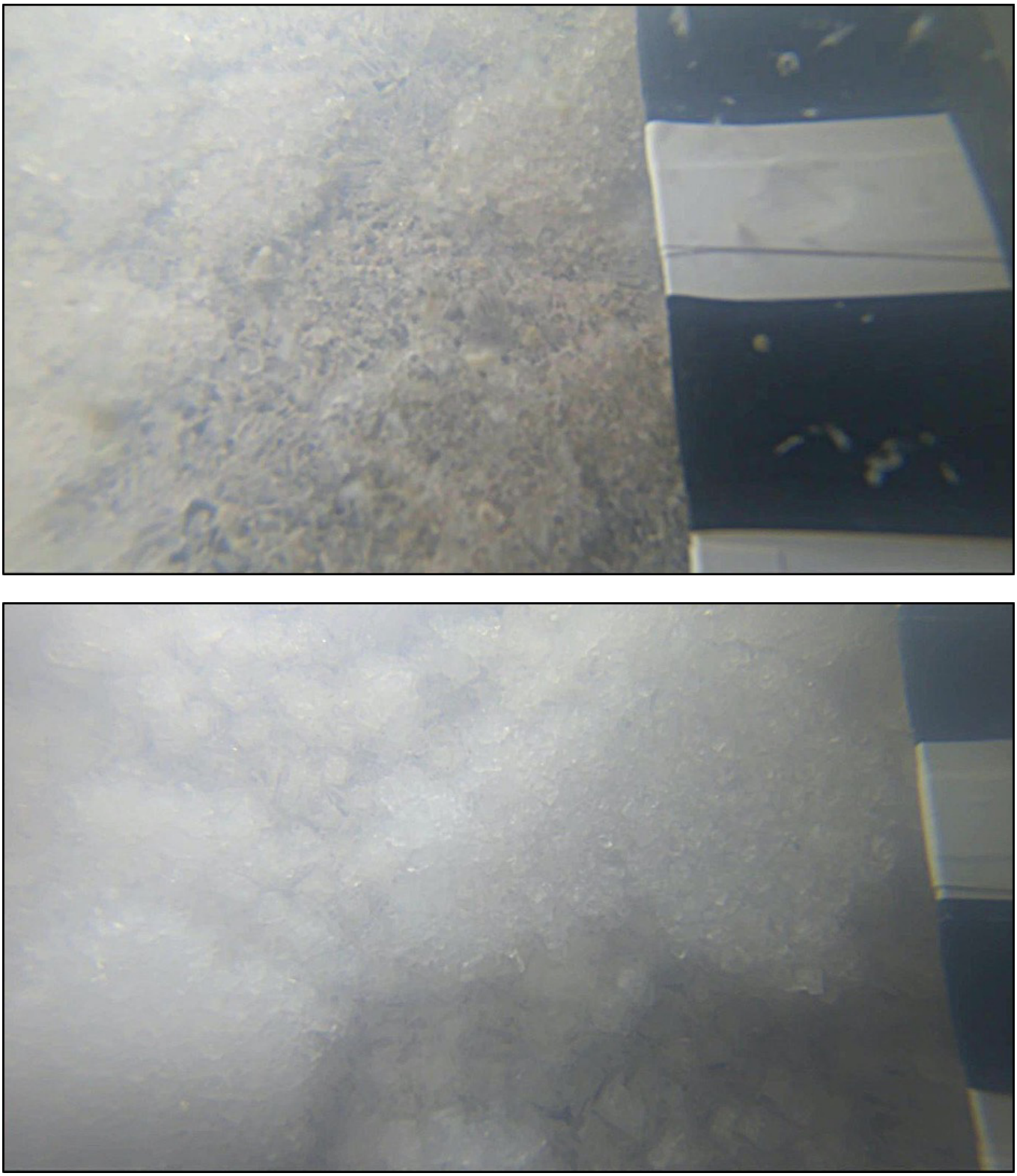

Figure 21. *Sunken salt rafts covering bottom growth halite crystals on the lake floor of the north arm. In both images, the patches of raised relief are halite cumulate rafts. Recently sunken rafts are finely crystalline such as in the bottom image. Sunken rafts serve as a growth site for coarser halite. (Top) Image captured near the Spiral Jetty at a water depth of about 10 ft on September 2, 2020. (Bottom) Image captured at site RD2 at a water depth of about 16 ft on September 23, 2020. Scale on right is in inches.*

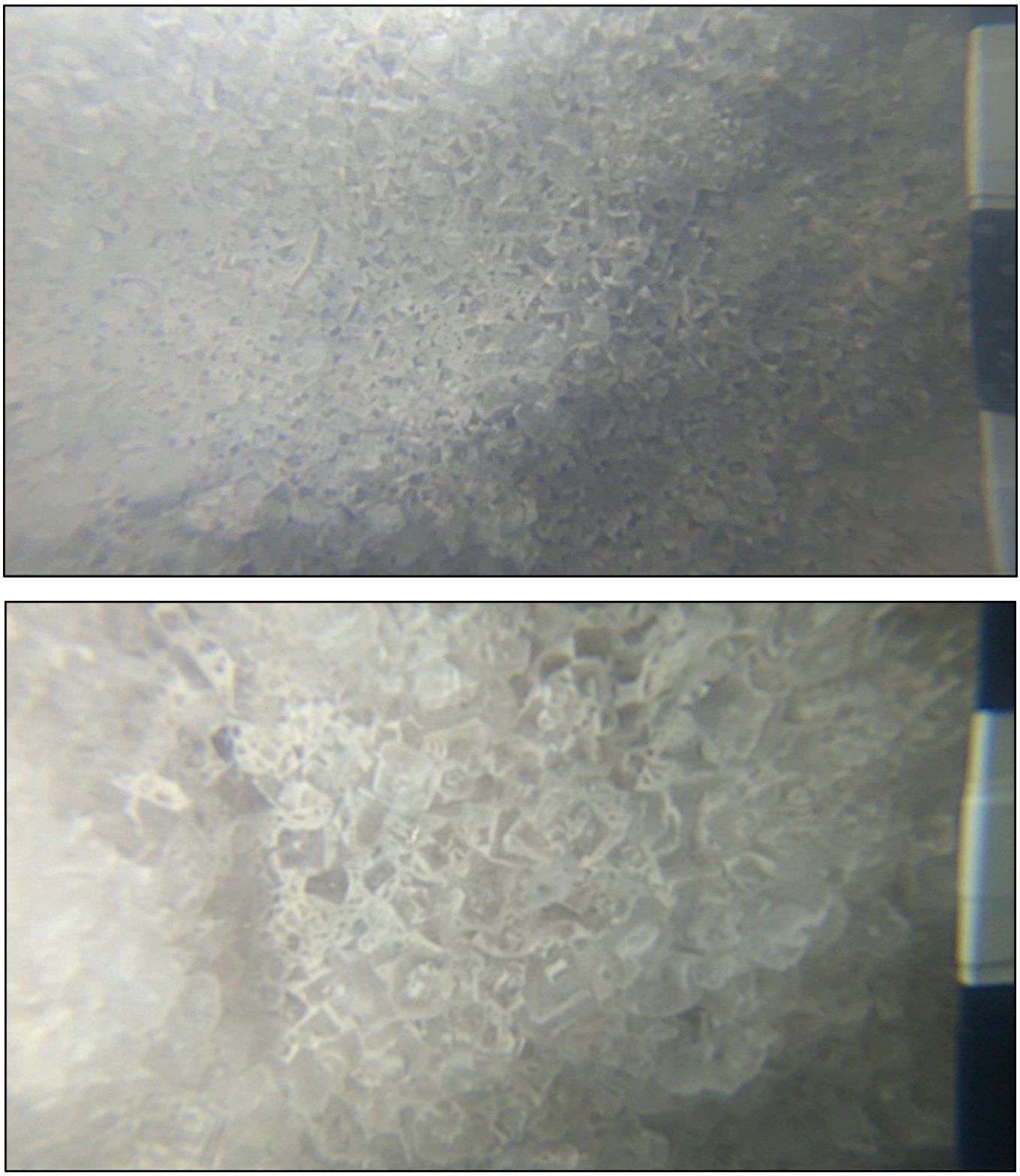

Figure 22. *White, chalky residue partially coating coarse bottom growth halite crystals on north arm lake floor. Top image captured at site LVG4 at a water depth of about 19 ft on September 23, 2020. Bottom image captured at site RD2 at a water depth of about 16 feet on May 25, 2021. Scale on right is in inches.*

Figure 23. *Exposed salt crust in the north arm above the water level. The crust is a smooth, planar dissolution surface of interlocking halite crystals. The planar surface is similar to that observed on the lake bottom salt crust during summer 2019 (figure 16). This photograph was taken during the summer of 2015. Pen for scale.*

they provide evidence of possible groundwater contribution at depth in the north arm or upwelling of less saline brines. Coincidentally, the LVG4 site is in proximity to an interpreted Quaternary fault (figure 1) that may serve as a potential conduit for groundwater flow. This is a significant observation for the occurrence of dissolution pipes forming within the lake at depth, considering they are typically reported to form subaerially when exposed to meteoric waters.

Buoy Systems

As noted above, buoy systems were deployed at the causeway on August 1, 2019, and at the Spiral Jetty on August 14, 2019, and September 2, 2020. On subsequent visits to the causeway and the Spiral Jetty on August 4, 2019, and October 24, 2019, respectively, the weighted lines were examined and they were completely clean with no halite precipitation at any depth. Based on observations from Rupke and others (2016) and Rupke and Boden (2020), the seasonal period for which the buoy systems were deployed is during the time when halite precipitation would occur (at least in nearshore environments). As previously noted, a salt crust was also not precipitating in the nearshore during this period. Overall, these observations are consistent with the north arm being undersaturated with respect to halite during the 2019 summer and fall seasons. In contrast, Sirota and others (2017) observed macro-crystalline halite growth on deployed lines during times when the Dead Sea was at supersaturation with respect to halite. Our buoy systems deployed in 2019 had drifted from their initial positions when examined and were gone when revisited in June 2020, likely due to storm events. We were unable to locate the buoy deployed on September 2, 2020, in late 2020, but we did locate and examine it in late May 2021. At that time, halite rafts were actively forming on the lake surface (figure 27A) and small halite crystals were beginning to form on the entire length of the buoy line, suggesting that the lake and water column was supersaturated (figure 27B). Although the halite growth was insufficient to take a meaningful measurement and buoy anchor was not yet cemented to the lake bottom. However, it was evident that clear bottom growth halite was actively forming (figure 27C).

Water Profile Measurements

During September 2019 and May 2021, we deployed the Hydrolab MS5 mini sonde to collect water profile information including temperature, turbidity, and depth at the north arm sites LVG4 and RD2. Figure 28 is representative of LVG4 on a hot, calm day—September 12, 2019—when the lake was undersaturated with halite and on a cool, overcast, slightly breezy day—May 25, 2021—during halite saturation. The September 2019 temperature and density profiles show an example of a thermally and chemically stratified meromictic lake (figures 28 and 29) (Stewart and others, 2009), although the temperature values only vary by a few tenths of a degree (figure 28). The temperature profile shows the epilimnion or lake surface

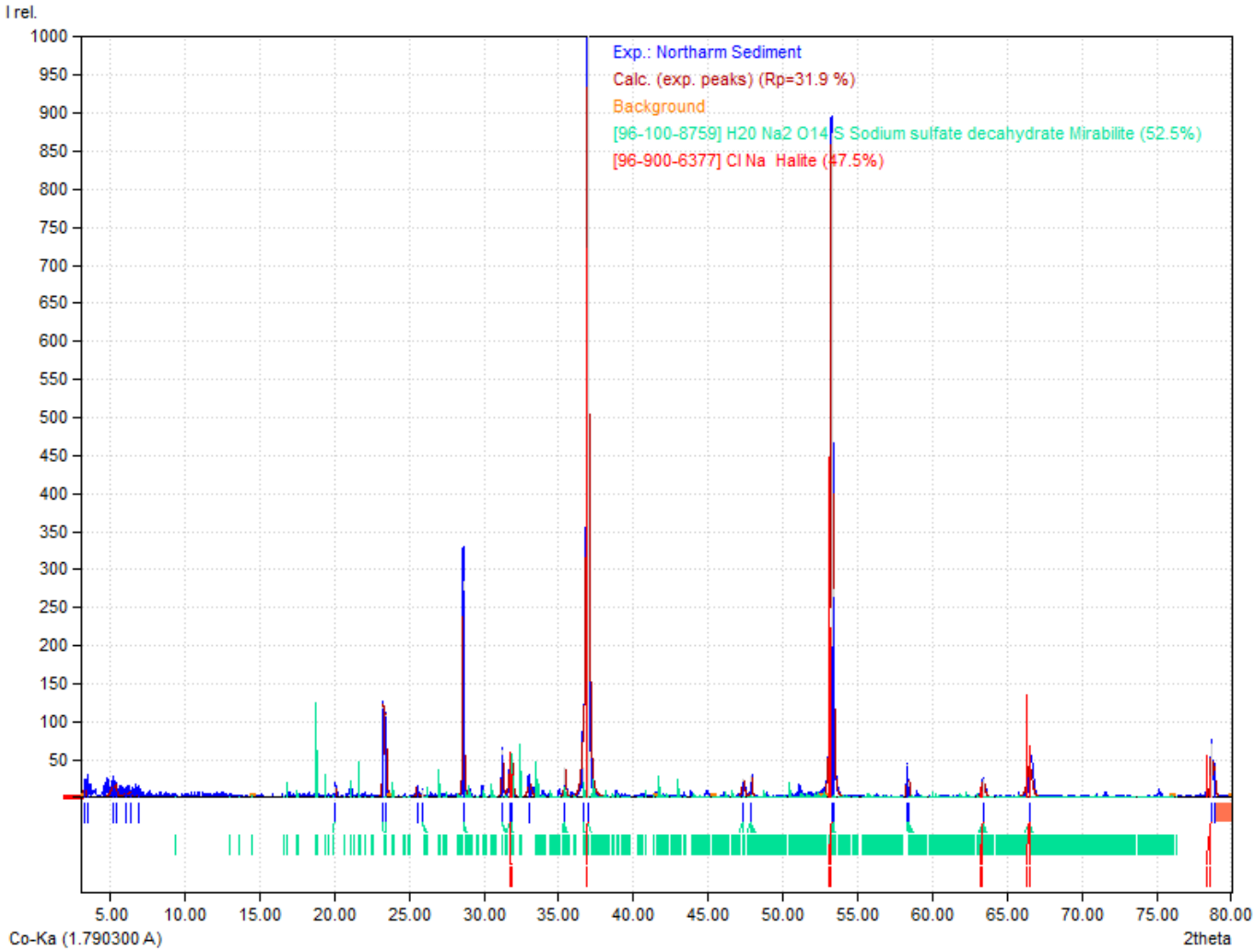

Figure 24. *X-ray diffraction pattern of a halite mixed sulfate sample retrieved from the lake substrate at 15 ft, RD2 location, north arm, Great Salt Lake. X-axis is the degree of 2theta and y-axis is relative peak intensity. The most intense peak heights are identified as halite (red). Mirabilite (green) or an unknown sulfate phase overlaps halite peaks and less intense peak heights. "Calc. (exp. peaks)" refers to an unknown reference pattern.*

is the warmest layer. The hypolimnion at water depth of 10 ft shows a slight decrease in temperature and the monimolimnion at bottom depth of 18 ft shows a slight increase in temperature. The density profile, measured at ~20°C in the lab, has a similar trend as the temperature profile and the highest density measurement is from the lake floor at 1.2208 g/cm^3, suggesting that this slight increase may represent a thin chemocline boundary. Turbidity, measured in nephelometric turbidity units (NTU), trends in a stepwise progression with depth and subtly reflects the thermal boundaries of the water column: low turbidity in the epilimnion followed by an increase at the metalimnion (~4 ft depth), followed by an increase in turbidity in the hypolimnion (12 ft depth). The increase in turbidity is related to particle accumulation in the water column as a mixture of chemical precipitates and plankton (eukaryotes, microbes) or organic debris (dead brine shrimp). The combination of these parameters suggests some type of thermal and chemical stratification with a lake bottom that has higher salinity. However, based on the small density gradient within the water column and applying the Brunt-Väisälä density buoyancy frequency equation (Anati, 1997), a windy storm event can quickly destabilize and mix the column. Therefore, storms and wind likely play a major role in mixing less dense epilimnion waters with the lake bottom.

The water profile for LVG4 on May 25, 2021, shows an opposite trend for temperature and density compared to September 2019, but turbidity shows a roughly similar trend (figure 28). The weather was cool, overcast, and breezy. The epilimnion lake surface temperature was ~17°C with a density of 1.219 g/cm^3 at 20.0°C with no obvious halite rafts, and the change in temperature throughout the water column was not as significant in comparison to the higher lake temperatures reported in September 2019. The absence of halite rafts on the water surface may be attributed to wind mixing or that the location is closer and directly north of the new causeway breach. The metalimnion/hypolimnion had only a slight increase in temperature by about 0.2°C coinciding with an increase in density (1.223 g/cm^3 at 20.0°C) and the monimolimnion cooled back to ~17°C while the lake bottom density increased to near

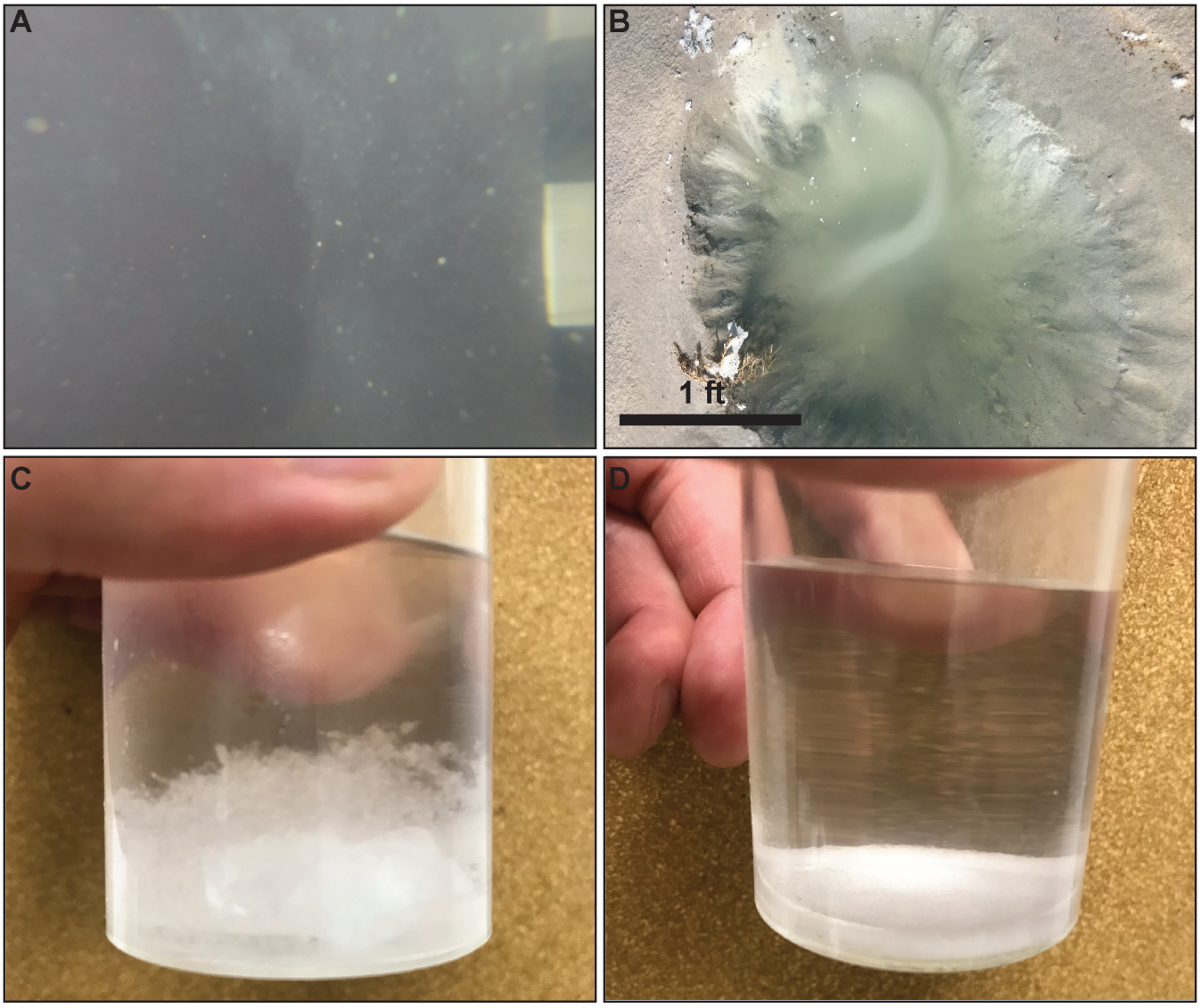

Figure 25. *Turbidity and mineral precipitation in north arm lake brine and groundwater.* ***A)*** *Underwater image showing white cloudy turbidity commonly observed in the water column of the north arm that may be a chemical precipitate or biological debris. Photo taken at an unknown depth.* ***B)*** *Cloudy turbidity of microcrystalline mirabilite forming in a spring seep hole from the south arm mudflat of White Rock Bay, Antelope Island (south arm).* ***C)*** *and* ***D)*** *Temperature and salinity experiment for a vial of a halite-saturated north arm lake brine at 32% salinity. C) Brine cooled to 0°C for 24 hours. Clear bladed mirabilite crystals (millimeter size) precipitated and lowered the salinity to 29.8%. D) After the brine was left at room temperature (~ 20°C) for several hours,the mirabilite crystals dehydrated and a white, milky mush formed, probably thenardite. The salinity raised back again to 32%.*

halite saturation (1.223 g/cm^3). Halite supersaturation at the lake bottom is implied by the presence of a coarsely crystalline halite crust documented by underwater imaging (figure 22); however, the cooling of bottom waters may be related to upwelling groundwater as indicated by halite dissolution pipes/holes (figure 26). The other possibility for a different temperature profile could be related to wind mixing the water column at the time of measurement.

At the RD2 sampling site on May 25, 2021, the weather conditions were calm with a surface lake temperature of ~16.8°C and halite rafts were actively forming. The site is roughly 3 miles from our buoy location offshore from the Spiral Jetty where halite was precipitating throughout the water column. The temperature profile had a similar trend to LVG4 where an increase in temperature occurred at ~5 ft in the metalimnion/hypolimnion by again only 0.2°C, followed by a decrease in temperature near the lake bottom close to ~16°C (figure 30). Density measurements showed the entire water column was at 1.223 g/cm^3 (at 20.0°C), or halite saturation. The turbidity at RD2 was substantially higher than at LVG4, even at the lake surface with a NTU of 14.1. The profile has a zigzag appearance possibly related to the halite rafts forming on the lake surface and foundering within the water column, with an increase to 14.5 NTU at ~5 ft coinciding with a peak temperature of ~17.2°C, followed by a decrease of 11.2 NTU at ~7 ft that correlates to decreasing temperature, and another increase to 14.5 NTU at lake bottom (figure 30).

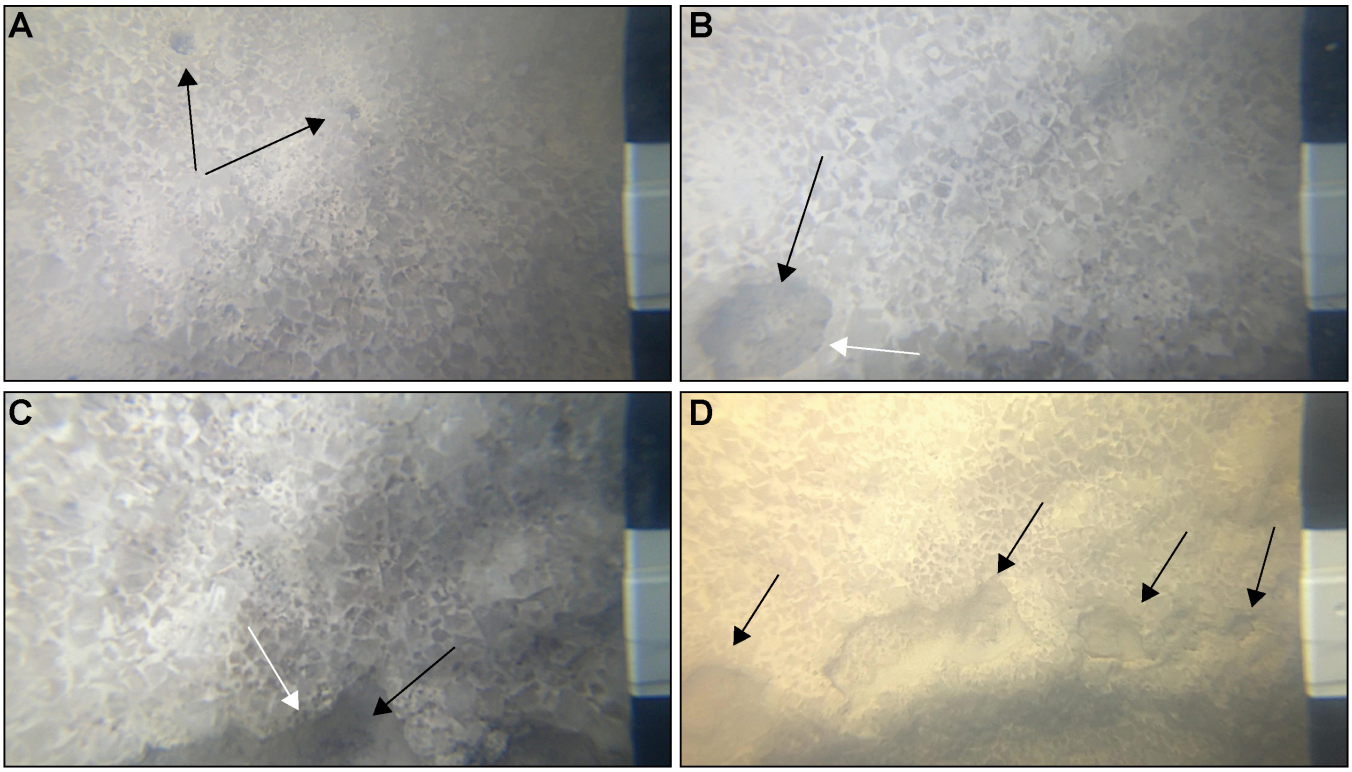

Figure 26. *Cavities in bottom growth salt crust of the north arm at site LVG4. The cavities likely represent dissolution pipes and holes from groundwater upwelling. Images are from May 25, 2021.* ***A)*** *Small, round, and isolated pipes (black arrows).* ***B)*** *Larger round dissolution hole (black arrow) with a faint rim (white arrow) suggestive of halite dissolution and recrystallization.* ***C)*** *Stark relief may indicate dissolution (and collapse?) due to groundwater upwelling. Note slight smoothness of the cavity edge (white arrow).* ***D)*** *Elevated view of (C) showing irregularly shaped dissolution cavities in a roughly linear arrangement. Scale on right is in inches. For images A, B, and D the camera cage is above the lake floor so features are larger than the scale indicates.*

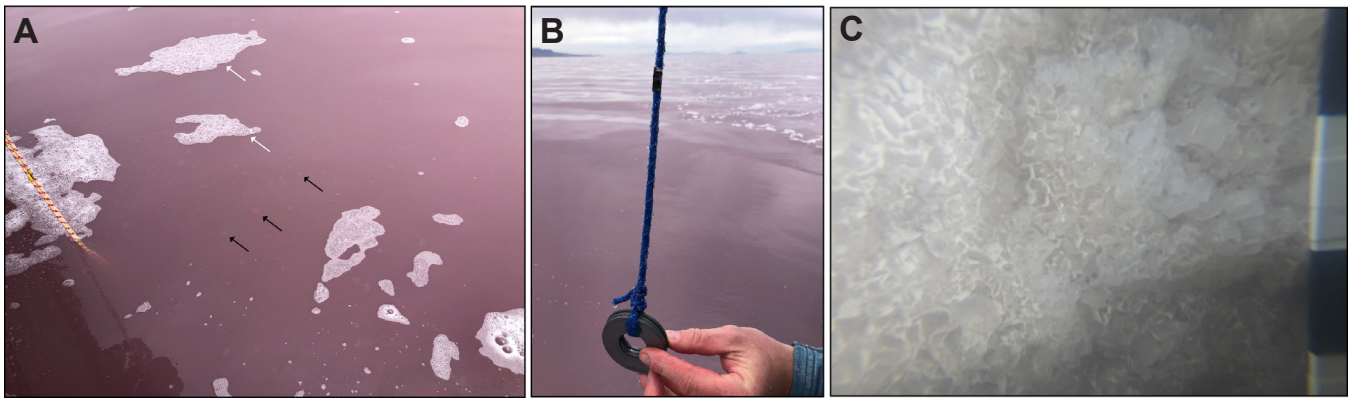

Figure 27. *Halite saturation and accumulation at buoy site located offshore from the Spiral Jetty on May 25, 2021.* ***A)*** *Image showing sub-inch size halite rafts (black arrows) and white foam (white arrows) floating on the lake surface.* ***B)*** *Salt accumulation rope connected to the buoy down to the lake bottom. The entire line had a thin halite crust coating indicating the entire 7 ft water column was halite saturated.* ***C)*** *Image of bottom growth halite crust next to the buoy. Scale on right is in inches.*

In summary, water column profiles from LVG4 represent two different seasonal conditions, one in late summer with no wind on a sunny, hot day and the other during the spring with windy, overcast, and cooler temperatures. The location of LVG4 is in the central part of Gunnison Bay where predominant winds from the northwest intersect along the fetch (figure 1). We consider it possible that on May 25, 2021, the temperature profile captured a lake turnover or thermal destabilization. The lack of halite rafts may be a result of wind disrupting the lake surface and not allowing for stable conditions or that the proximity to the new breach (about 7 miles) is controlling halite saturation by less dense inflow waters. For both measurement periods the density of the surface layer at LVG4 was below 1.220 g/cm^3 (at ~20°C) or undersaturated with respect to halite. The RD2 site is more sheltered from the fetch and farther north of the breach (about 15 miles) where halite raft accumulation was observed. The temperature profile shows a similar trend to that of LVG4 and may represent water column thermal mixing despite the density being constant at depth at 1.223 g/cm^3 (at 20.0°C), including the near-surface sample.

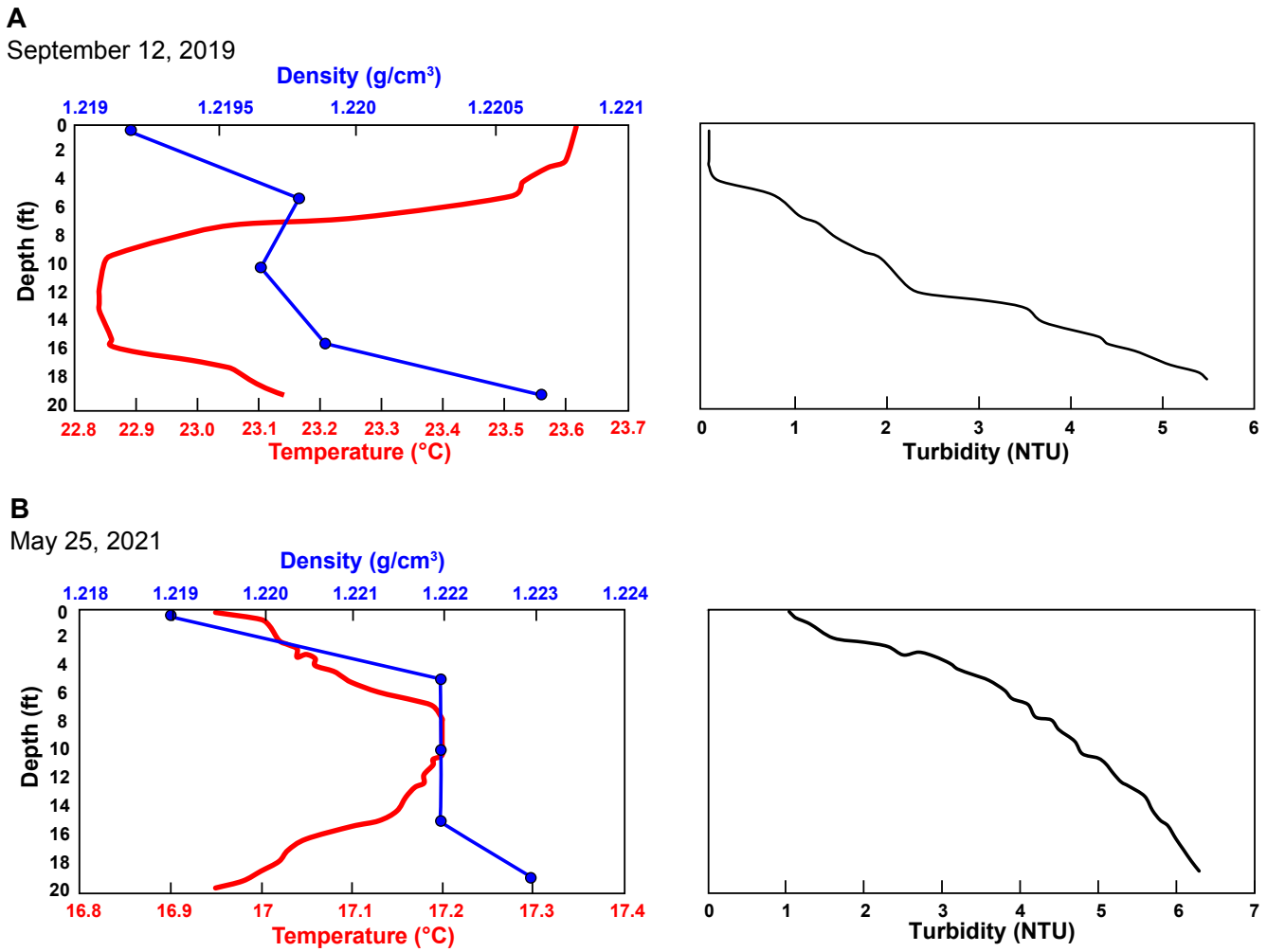

Figure 28. *Water column profiles at the LVG4 site on September 12, 2019 (A) and May 25, 2021 (B).* ***A)*** *September 9, 2019, was a calm, hot day and May 25, 2021, was cool, cloudy, and slightly breezy. Density sample points (blue) were measured in the lab at 20°C. Temperature (red) and density points somewhat trended similarly with depth except at the epilimnion surface. The profiles suggest a thermally and partially chemically stratified meromictic lake during this time (see figure 29). The lake brine did not appear to be at halite saturation and the salt crust was coated with a white sediment and had partial truncation. Turbidity increased with depth (NTU - nephelometric turbidity units) in a stepwise pattern with the largest increase coinciding around 12 ft where the density began to increase towards the bottom, possibly indicating a chemocline or particulates in the water column.* ***B)*** *May 25, 2021, the temperature profile (red) trends opposite when compared to September 12, 2019, and the density sample points are similar but reach higher densities (1.222 g/cm^3) at shallower depths. The increase in density overlaps with increasing temperature and increases at the monimolimnion as temperature decreases. The cooler bottom temperatures may reflect upwelling of colder groundwaters as indicated by dissolution holes in the bottom growth halite crust. The epilimnion has the lowest density and no halite cumulate rafts on the surface were observed at the site. The turbidity increases broadly with depth with a steeper slope at the base of the epilimnion. Because LVG4 is closer to the causeway breach, less dense south arm inflow waters may be surfacing at the epilimnion.*

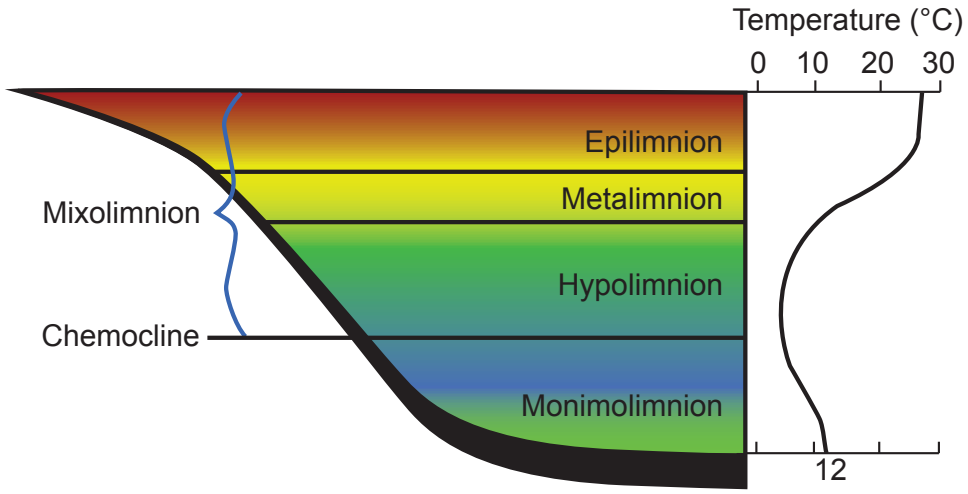

Figure 29. *Schematic of a typical meromictic lake (after Stewart and others, 2009). Note the chemocline boundary is below the mixolimnion and begins where temperature slightly increases near the bottom of the lake (monimolimnion). Bottom lake temperature is 12°C shown in this example (bottom x-axis).*

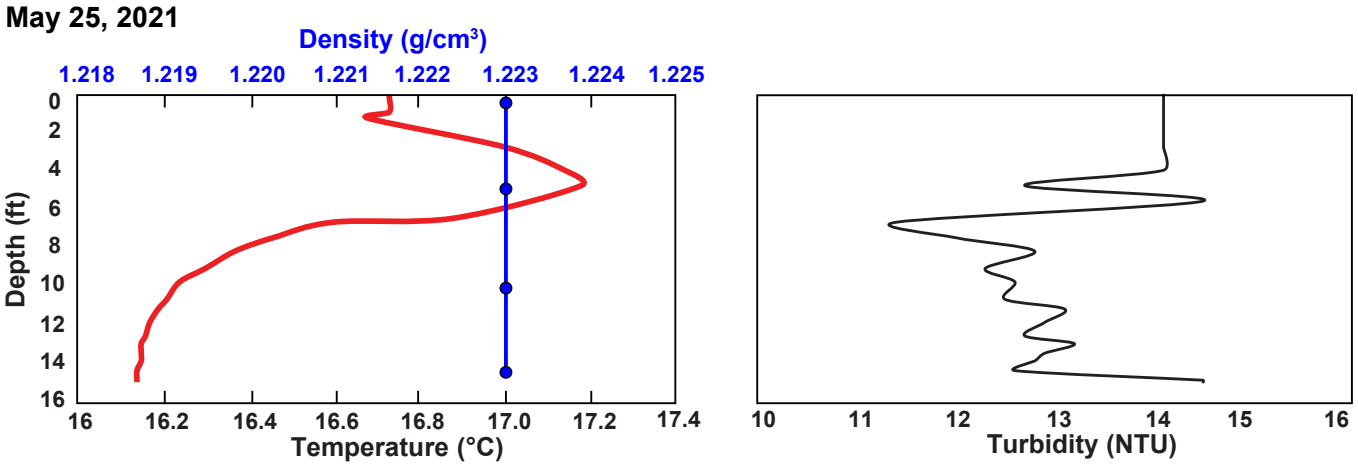

Figure 30. *Water column profile of RD2 on May 25, 2021. The temperature (red) profile shows thermal stratification for this site location. Temperature increases below the epilimnion in the metalimnion and progressively decreases into the monimolimnion. Density remains constant throughout the water column at halite saturation (density of 1.223 g/cm³) and halite rafts on the lake surface were observed. The turbidity (NTU - nephelometric turbidity units) is much higher at this location than at LVG4 and shows a zigzag trend probably due to halite supersaturation and the foundering of halite rafts throughout the water column. Interestingly, there is a turbid zone associated with peak temperature and may reflect a chemocline where halite rafts are collecting in suspension.*

Density Experiments

Density experiments revealed interesting results for north arm brine that was sampled from the Spiral Jetty in November 2019 (table 4). At all temperatures, except for 0°C, the difference between the "spiked" and "control" brine densities indicated that the north arm is undersaturated with respect to halite. In fact, all empirical degrees of halite saturation (EHS) were negative and below 10 σkg/m^3. The spike brines containing 10 g NaCl had densities above 1.220 g/cm^3 except for the sample at 49°C and all lake brine control samples were below 1.220 g/cm^3 (table 5). The results for the experiment at 0°C had subtle differences and the lowest densities (spike: 1.1961 g/cm^3; control: 1.1972 g/cm^3), therefore the EHS was only 1.1 σkg/m^3 (figure 31, table 5). At such low and similar densities (i.e., salinity), this EHS value is not definitive regarding saturation state. We also observed that mirabilite precipitated in both the spike and control samples at 0°C which implies its formation at low temperatures has an impact on the physico-chemical conditions of the north arm lake brine. This is significant because it shows temperature and the formation of mirabilite may play a role in controlling EHS during different seasons.

For the remainder of the project, we performed a simpler version of this experiment by measuring the density of north arm brine samples and NaCl-spiked north arm brine samples (appendix D). When the spike density was notably higher than the control (EHS values below -1), the north arm was undersaturated. However, when the density differential was minimal or the control density was higher than the spike (EHS above -0.6), we considered the north arm to be supersatu-

Table 4. *North arm brine composition measured from three different laboratories from samples collected on November 16, 2019. For the first two rows, the density was measured by UGS and the ions and TDS were measured by the noted laboratory.*

Laboratory	Density (g/L)	Na^{+} (g/L)	Mg^{+2} (g/L)	K^{+} (g/L)	Li (g/L)	Ca^{+2} (g/L)	Cl^{-} (g/L)	SO_4^{-2} (g/L)	TDS (g/L)
UGS: American West Analytical Laboratories	1.211	93.6	11.8	11.2	N/A	0.3	180.0	23.9	321
UGS: Chemtech-Ford	1.211	86.8	12.2	7.4	N/A	0.3	181.0	24.6	312
US Magnesium: Control Lab[1]	1.212	100.6	12.1	7.7	0.03	0.4	177.9	25.2	324

[1] Calculated values from reported density and % weight of brine.

Table 5. *Temperature and density experiments for measuring the degree of halite saturation, north arm brine, November 16, 2019.*

Sample	T (°C)	Density (g/cm^3)	Density ($\sigma kg/m^3$)	Pure water (kg/m^3)	EHS*	Saturation state
Spike 10 g NaCl	49 °C	1.2164	227.9119	988.48	-13.5	undersaturated
Control	49 °C	1.2029	214.4119			
Spike 10 g NaCl	22.3 °C	1.2200	222.300	997.70	-18.5	undersaturated
Control	22.3 °C	1.2015	203.800			
Spike 10 g NaCl	21.3 °C	1.2206	1220.6	997.90	-11.7	undersaturated
Control	21.4 °C	1.2089	211			
Spike 10 g NaCl	4.4 °C	1.2214	221.430	999.97	-11.9	undersaturated
Control	4.4 °C	1.2095	209.53			
Spike 10 g NaCl	0 °C	1.1961	196.26	999.84	1.1	saturated?†
Control	0 °C	1.1972	197.36			

*EHS is the empirical degree of halite saturation recorded in sigma units (σkg/m3) that is calculated by subtracting the reference density of pure water at the same temperature.

†Mirabilite precipitated in control and spike samples, lowering brine density and affecting halite saturation.

rated. Overall, the experiments show that the north arm brine was undersaturated (with respect to halite) in 2019 and the first half of 2020, became saturated during the summer of 2020, was unsaturated again in late 2020/early 2021, and became saturated again in late May 2021. These measurements are in general agreement with our other observations in the nearshore environment as well as our images at depth.

Based on our experiments we infer an approximate halite saturation density of 1.223 g/cm^3 at 20°C. However, the experiments suggest that saturation density may fluctuate to some degree given that our measured spike densities ranged from 1.217 to 1.225 g/cm^3 at ~20°C and our measured control densities ranged from 1.222 to 1.225 g/cm^3 at ~20°C when the lake was considered to be saturated.

Interestingly, during the precipitation of mirabilite at low temperatures near 0°C, the density of the lake brine was low at room temperature (1.202 g/cm^3 at 22.3°C) (table 5), suggesting that precipitation of mirabilite (along with temperature) affect brine density and possibly halite saturation. We tested this with another experiment from halite-saturated lake brine collected nearshore at the Spiral Jetty on June 5, 2021. A handheld refractometer was used to measure the salinity at a room temperature of ~23.0°C and measured 32% salinity. About 50 mL of the brine was placed in the freezer for one day and formed mirabilite (figure 25C). The salinity of the brine decreased to 29.8% at 0°C, confirming that the precipitation of mirabilite lowers brine salinity.

Geochemistry of Lake Brine and Spring Seeps

The composition of north arm lake brine sampled from the nearshore of the Spiral Jetty on November 16, 2019, (table 4) was evaluated for mineral saturation states, primarily halite, using the computer program PHRQPITZ. This brine composition was collected during this time because it was a period of halite undersaturation based on field observations and density measurements, and we also wanted to understand when north arm brine is saturated with halite at different tempera-

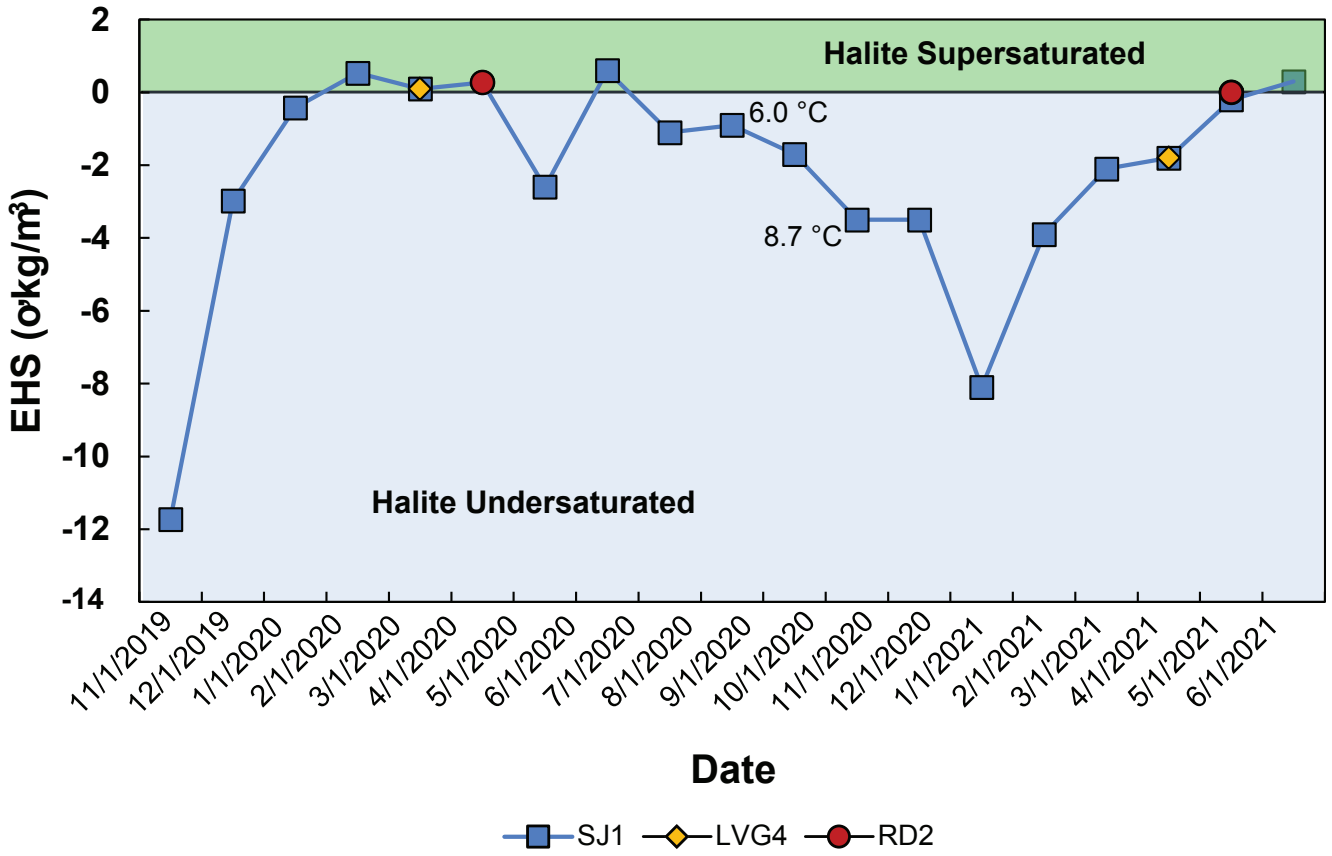

Figure 31. *Halite saturation as determined by density tests during the study period. A negative value for the empirical degree of halite saturation (EHS in sigma units) indicates undersaturation and a positive EHS indicates supersaturation. All measurements were made at room temperature (~ 20°C) unless otherwise noted to reflect lake temperature.*

tures and during evaporative concentration. The composition used was measured by U.S. Magnesium Corp.'s control laboratory (table 4). The Q/K (ion activity product, Q, divided by equilibrium constant, K, =1) is used to calculate mineral saturation states and a value of 1 indicates a brine is saturated for a particular mineral and precipitation occurs; below this value minerals are undersaturated. Modeling the brine at temperatures between 0°C and 40°C confirms, to some extent, that the density experiments were of true value showing that at low temperatures (<5°C) mirabilite (and even gypsum) are saturated in the Na-Cl-SO_4 system (figure 32A). Experimental studies have shown mirabilite is stable up to ~32°C depending on percent relative humidity (~83%) and high concentrations of Na_2SO_4 (~500 g/L) (Marliacy and others, 2000; Genkinger and Putnis, 2007); however, PHRQPITZ's evaporation simulation operates under dry conditions (no humidity) and does not perform well to speciate Na_2SO_4 (thenardite). Halite was undersaturated with a Q/K value of 0.89 (a value of 1 Q/K is at saturation) and becomes slightly more undersaturated with increasing temperature. Also shown in figure 32A are the concentrations (grams) of Na^+ and SO_4^{2-} species. Na^+ and SO_4^{2-} decrease in concentration and are sequestered when mirabilite forms. Evaporating 1 kg of the brine at 25°C also concludes that the system was initially undersaturated with halite (figure 32B). After 0.10 kg of water loss, halite precipitates. This precipitation can be illustrated by observations made in the lab by taking 1 kg of lake brine and exposing it to the atmosphere for one day. After some water loss by evaporation, the lake brine precipitated halite. Results from this modeling suggest the north arm lake brine, at densities below 1.223 g/cm^3 (at 20°C), is not saline enough to precipitate halite until 10% of the water has evaporated. Fluctuations of fresher input waters (meteoric precipitation, run-off, possibly groundwater) and possibly the mixing of less saline south arm brine may contribute to sustaining an undersaturated halite north arm lake brine.

The objective to collect groundwater samples was to 1) measure and analyze their ionic compositions and stable isotope ratios (δ^2H and $\delta^{18}O$) to determine if a chemical gradient from lake margin to nearshore exists, 2) investigate mineral saturation states via computational evaporation modeling, and 3) compare compositions and isotopic results with other lake margin groundwater sources measured by Kirby and others (2019). Table 2 provides the analytical results for the groundwater samples and spring waters sampled from the northern part of the north arm in Spring Bay and Locomotive Springs. Springs near the Spiral Jetty are more dilute with lower proportions of ion concentrations than groundwaters along the mudflat. Indeed, the transect of groundwater piezometers showed an increasing gradient of brine concentration from the lake margin towards the shore (table 2). Groundwater closer to the shore has a composition similar to that of the north arm brine (e.g., piezometers SJP5 and SJP6). Evapo-

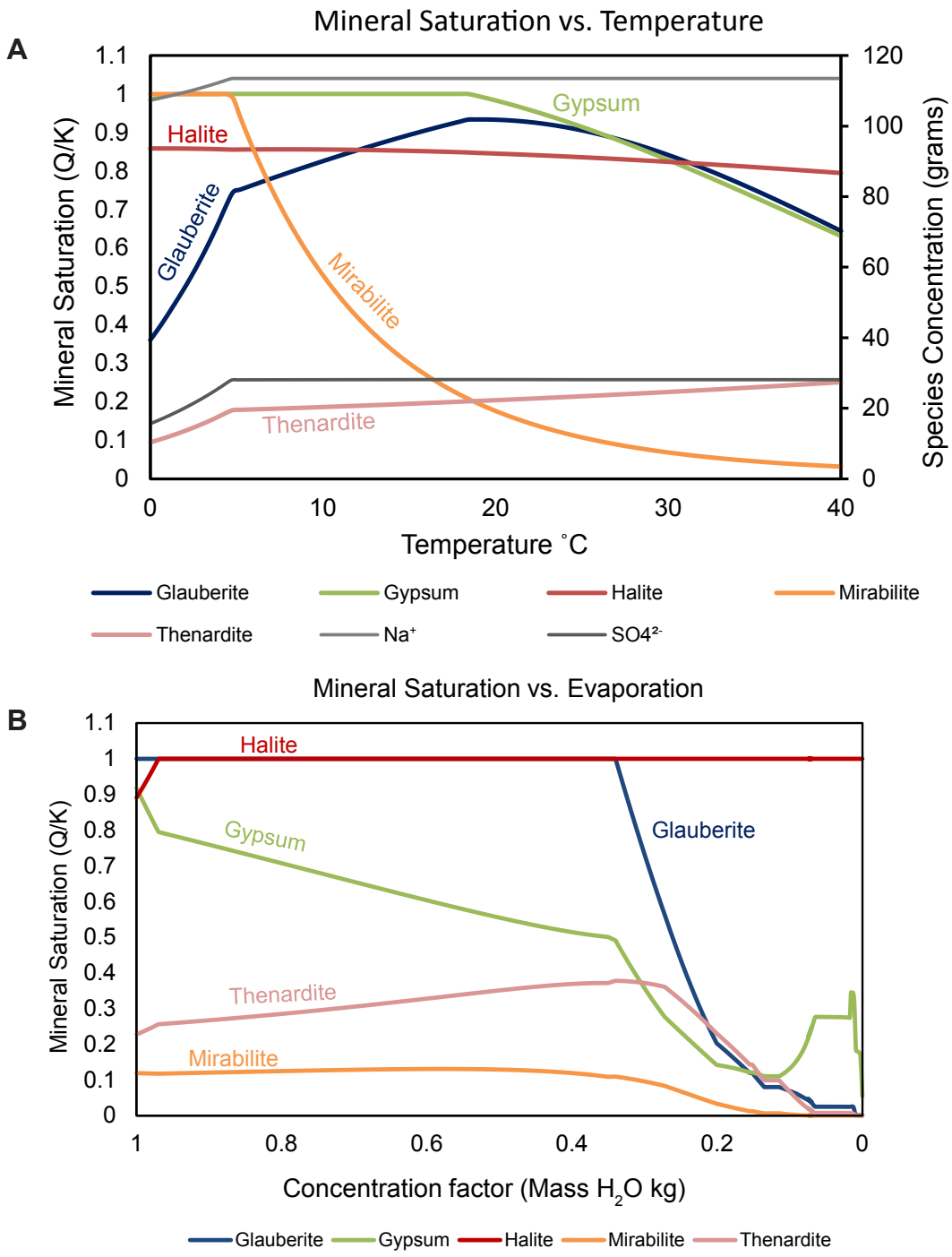

Figure 32. *Model of brine evolution for north arm water and saturation states (Q/K) for typical mineral assemblages controlled by temperature and evapoconcentration. The brine was sampled on November 16, 2019, nearshore Spiral Jetty and the chemical composition was measured by U.S. Magnesium Corp.'s control lab (table 2). The computer program PHRQPITZ was used to model Q/K (ion activity product, Q, divided by equilibrium constant, K, =1) and mineral saturation or precipitation is shown as a value of 1; below this value the minerals are considered undersaturated.* ***A)*** *North arm brine composition simulated at temperatures of 0°C to 40°C. Gypsum (green line) and mirabilite (orange line) are initially saturated in the brine at low temperatures. Halite (red line) remains relatively constant as undersaturated (~0.89 Q/K) in the Na-Cl-SO_4 system while temperature changes. Glauberite (purple line) and thenardite (pink line) change in solubility states with respect to temperature but remain undersaturated. Note lower concentrations of Na^+ and SO_4^{2-} species (right y-axis) at colder temperatures during the precipitation of mirabilite.* ***B)*** *Simulated evaporation of north arm brine under open conditions at 25°C and atmospheric pCO_2 concentrations (400 ppm). Concentration for 1 kg H_2O/brine increases to the right (loss of water/evaporation). Glauberite precipitates initially during evaporation, removing Ca^{+2} from the brine, and halite eventually precipitates but at a concentration of ~0.89 kg or a loss of evaporated water of 0.11 kg. The computer program models glauberite to become undersaturated at higher concentrations and possible back reaction into the brine. This suggests that during November, north arm brines were undersaturated with halite due to net decrease in evaporation or lake brine mixed with fresher water input.*

ration modeling of the Spiral Jetty groundwaters and spring seeps produced similar sequences for mineral saturation states, where the dilute brines required more evaporation than concentrated brines closer to the lake. Figure 33 shows the minerals that will precipitate from the SJ4 spring seep (figures 6D and 12) from evaporative concentration. The first mineral to precipitate is dolomite or a carbonate phase followed by gypsum, magnesite ($MgCO_3$), and eventually halite and glauberite as the brine becomes more concentrated. The reason dolomite (or an unknown carbonate phase) precipitates first is that Ca^{2+}-Mg^{2+} and HCO_3^- are removed in a 1:1 ratio from the dilute brine. Because the brine is more concentrated with Mg^{2+} than Ca^{2+} the caveat of the computer program does not calculate thermodynamic properties for high or low Mg calcite and only calculates dolomite or magnesite, which may alter the evaporative brine evolution sequence. However, this sequence of mineral saturation states confirms our field observations of initial mineral precipitation near the spring discharge zone (carbonate, gypsum) and the residual halite brine that drains into the polygons. For comparison, the composition for water from Locomotive Springs, northwest of Spring Bay (table 2), was also evaluated for mineral saturation states and modeled for calculating the concentration of major ions at halite saturation. Locomotive Springs and the majority of springs around Spring Bay are less saline than the spring seeps at the Spiral Jetty, but eventually discharge into the north arm or mix with lake brine groundwater. Locomotive Springs has the highest discharge, is less saline, and its upstream meteoric source waters drain through volcanic rocks and basin fill (Hurlow and Burk, 2008; Kirby and others, 2019). Evaporation of the spring waters produced a similar mineral sequence compared to SJ4 where dolomite and gypsum precipitated first followed by magnesite and halite (figure 34A). At the evaporation step when halite precipitates, the calculated ion composition is close to that of a typical halite-saturated north arm brine (figure 34B), in terms of concentration of Na^+ and Cl^-. In summary, dilute groundwaters and spring seeps along the margins of the north arm appear to evolve into a brine that is capable of precipitating minerals similar to that of a north arm lake brine.

The utility of the stable isotope ratios of deuterium and oxygen-18 (δ^2H_{VSMOW} and $\delta^{18}O_{VSMOW}$, respectively) in groundwater permits interpretation of possible physical and chemical fractionation processes for water and water vapor, such as evaporation, condensation, diffusion, reaction between a solid and solution, and biological influences. Therefore, stable isotopes can be used as tracers for recognizing different fractionation pathways. Isotopic ratios for spring seeps discharging at the surface near the Spiral Jetty cluster as lighter, more depleted, ratios, whereas groundwater is slightly enriched (figure 35, table 2). Water from the well-known barite spring mound near Rozel Point groups with the spring seeps around the Spiral Jetty (data from Kirby and others, 2019). In com-

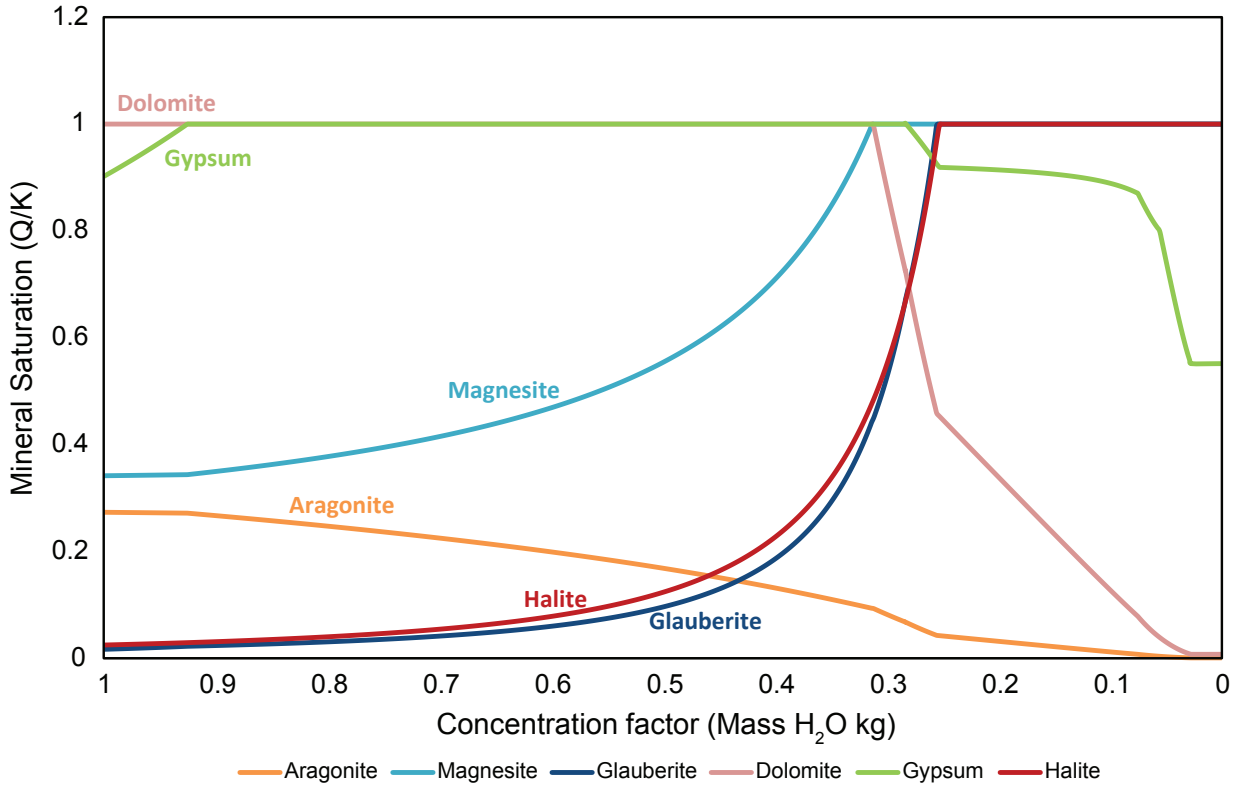

Figure 33. *Modeling of SJ4 spring seep waters and saturation states (Q/K) for typical mineral assemblages and sequence controlled evapoconcentration, at 25°C. Dolomite or a carbonate phase is initially at saturation followed by gypsum upon evaporation. Further evaporation produces magnesite and eventually halite and glauberite. Note after gypsum becomes undersaturated, halite precipitation occurs, reflecting chemical divides for the formation of a halite-saturated north arm lake brine. Aragonite is undersaturated because the computer program selectively favors the precipitation of dolomite and magnesite.*

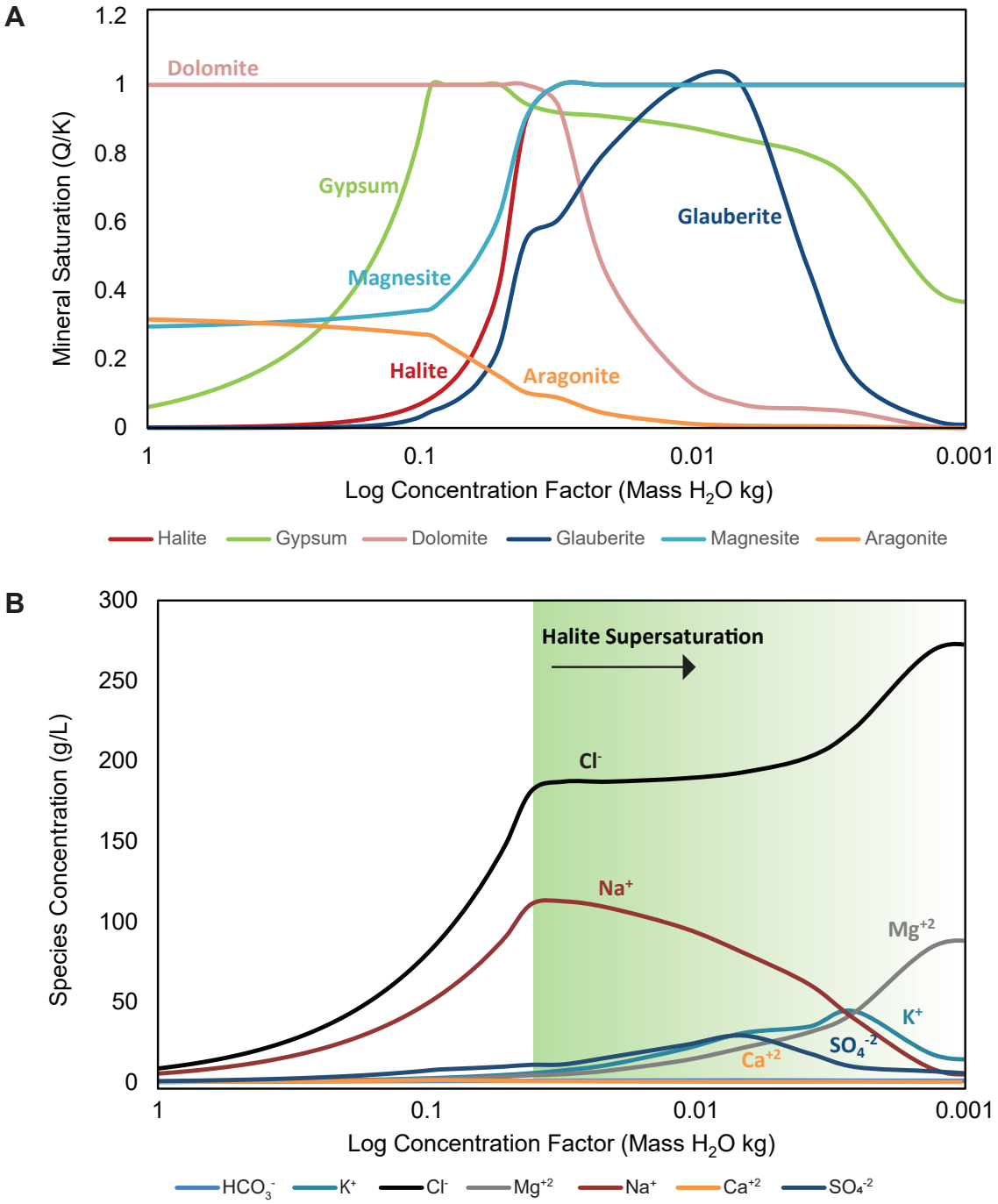

Site	Na^{+}	Mg^{+2}	K^{+}	Ca^{+2}	Cl^{-}	SO_4^{-2}	HCO_3^{-}
Modeled Locomotive Springs	112.67	5.01	7.45	0.51	187.15	11.16	1.08
North Arm brine 8/17/2020	114	13	7.94	0.34	200	26.7	0.3

Figure 34. *Modeling of Locomotive Springs waters and saturation states (Q/K) for typical mineral assemblages precipitated under evapoconcentration and calculated species at halite saturation.* ***A)*** *Evaporation of the dilute spring waters produces a similar sequence of mineral saturations as produced from SJ4 at the Spiral Jetty. Note concentration is in log form to show mineral precipitation from dilute spring waters.* ***B)*** *Speciation of ion concentrations (left axis) during evaporation of the dilute spring water. Table below shows calculated ion composition at the evaporation concentration step (green gradational shade) when halite supersaturation is reached. The calculated composition is similar to a halite-saturated north arm lake brine that was sampled on August 17, 2020.*

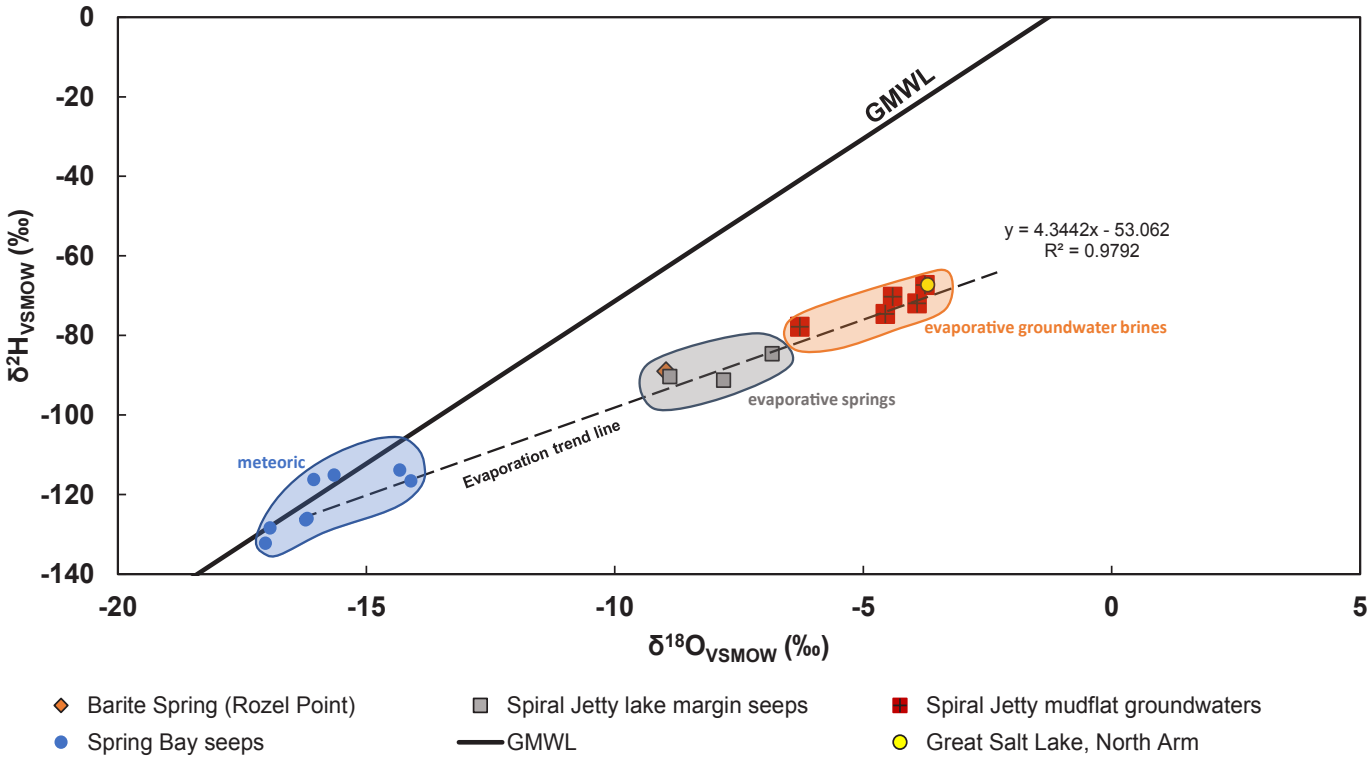

Figure 35. *Stable isotope ratios of deuterium (δ^2H) and oxygen ($\delta^{18}O$) measured in Vienna Standard Mean Ocean Water units (VSMOW) from spring seeps and groundwaters from the Spiral Jetty and spring waters from springs around Spring Bay and Locomotive Springs. The Spiral Jetty spring waters are lighter than mudflat groundwaters; mudflat groundwaters become increasingly heavy towards the lake shore. A positive covariance trend line diverges from the Global Meteoric Water Line (GMWL) (after Rozanski and others, 1993) from meteoric-influenced spring waters around Spring Bay and Locomotive Springs that is suggestive of an evaporation and possibly a chemical binary pathway.*

parison, fresher springs around Spring Bay are more enriched and fall along the Global Meteoric Water Line (GMWL) (Rozanski and others, 1993). The GMWL is the global average annual relationship between δ^2H_{VSMOW} and $\delta^{18}O_{VSMOW}$ from meteoric waters (i.e., rivers, lakes, rain, and snow); however, local water lines may differ as a result of different climatic and geographical factors. The more depleted stable isotope ratios from the Spiral Jetty groundwaters and spring seeps suggest evaporation and degassing of the waters has occurred and/or a combination of chemical mixing with different waters. Chemical precipitation may also be a driving factor for heavier isotopic ratios. The positive covariant trend, with a slope of 4.3442, diverging from GMWL is indicative of an evaporation pathway and possibly an endmember mixing line of groundwater mixing with north arm lake water. Stable isotope ratios for the north arm lake brine are depleted and similar in composition to near shore groundwater values, suggesting the extent of groundwater-lake water mixing (figure 35).

CONCLUSIONS

The results of this study show three transitions of the north arm brine saturation state from mid-2019 through mid-2021: 1) from undersaturated in the second half of 2019 through the first half of 2020 to saturated in the second half of 2020, 2) back to undersaturated in very late 2020 through most of the first half of 2021, and 3) to saturated in the late first half of 2021. These transitions and states were identified through nearshore observations, underwater photography, buoy observations, density measurements and experiments, and geochemical modeling. The undersaturated period from the second half of 2019 through July 2020 was identified by an absence of a salt crust on the nearshore lake floor, a smooth salt crust surface photographed at depth in the north arm, lack of precipitation on our buoy system, density measurements below what we have experimentally determined as saturation density, and geochemical modeling. The transition to saturation in August 2020 was marked by salt rafts on the lake surface, coarsely crystalline halite growth on the nearshore lake floor and at depth, sunken salt rafts at depth, and density measurements above our estimated saturation density. During the saturation period, which continued through at least late October, we recorded up to 3 inches of halite growth on the nearshore lake floor. Our images of coarsely crystalline halite growth at depth (up to about 25 feet) in the north arm indicate that the entire north arm water column reached halite saturation. Dissolution of the submerged nearshore salt crust and decreasing lake brine density accompanied a return to undersaturation in December 2020 through early May 2021. The final transition back to saturation in late May and June of 2021 was identified with salt rafts forming on the lake sur-

face, halite growth on the buoy line, patchy salt crust forming in the nearshore environment, and an increase in lake brine density to the saturation point. At depth, the salt crust had a rough, coarsely crystalline surface in late May.

Based on observations and experimentation during the study, we estimate the halite saturation density of the north arm to be approximately 1.223 g/cm^3 at 20°C. When our lake observations indicated saturation (such as brine surface salt raft formation and lake floor salt crust formation), density was close to that value. The density saturation experiments also suggest a similar value when the differential between the control and spike samples was small. Using this value, we estimate that the north arm becomes saturated at a salinity between 300 and 350 g/L using historical data (Utah Geological Survey, 2020). Where sufficient density data exist, we can also infer other times when the north arm has been saturated outside the time window of this study (figure 36). Clearly, saturation can be a seasonal phenomenon so collecting lake brine density data at a sufficiently short time interval (quarterly at a minimum) has value.

Since the opening of the new causeway bridge in December 2016, density measurements suggest that the north arm approached saturation in late summer 2017 and 2018 (figure 36), but accompanying observations from 2017 showed minimal halite precipitation. We consider it likely that if saturation was reached in 2017, it was only for a brief time allowing minimal halite precipitation. Halite saturation appears to have been reached in late summer 2018, but we have no record of whether a substantial crust was precipitated at that time, especially during mid-late summer. Since no halite saturation occurred in 2019, 2020 may have been the first significant halite precipitation to occur since the bridge opening. We find it notable that in 2020, the north arm did not reach halite saturation until August, but in 2021 had already reached saturation by late May. Halite saturation is certainly a function of lower lake level, but may also be due to the north arm approaching hydrologic equilibrium following the bridge opening; however, it appears that the initial inflow of less saline south arm waters diluted the north arm brine and that there was a 1- to 2-year lag, at minimum, for reestablishing significant halite saturation in conjunction with lower lake levels.

Groundwater discharge near the lake margins and nearshore environments appears to influence dissolution of the halite crust and the inflow of solutes that evolve to a lake brine chemistry. The contribution of groundwater to the north arm brine system is still not well understood or constrained

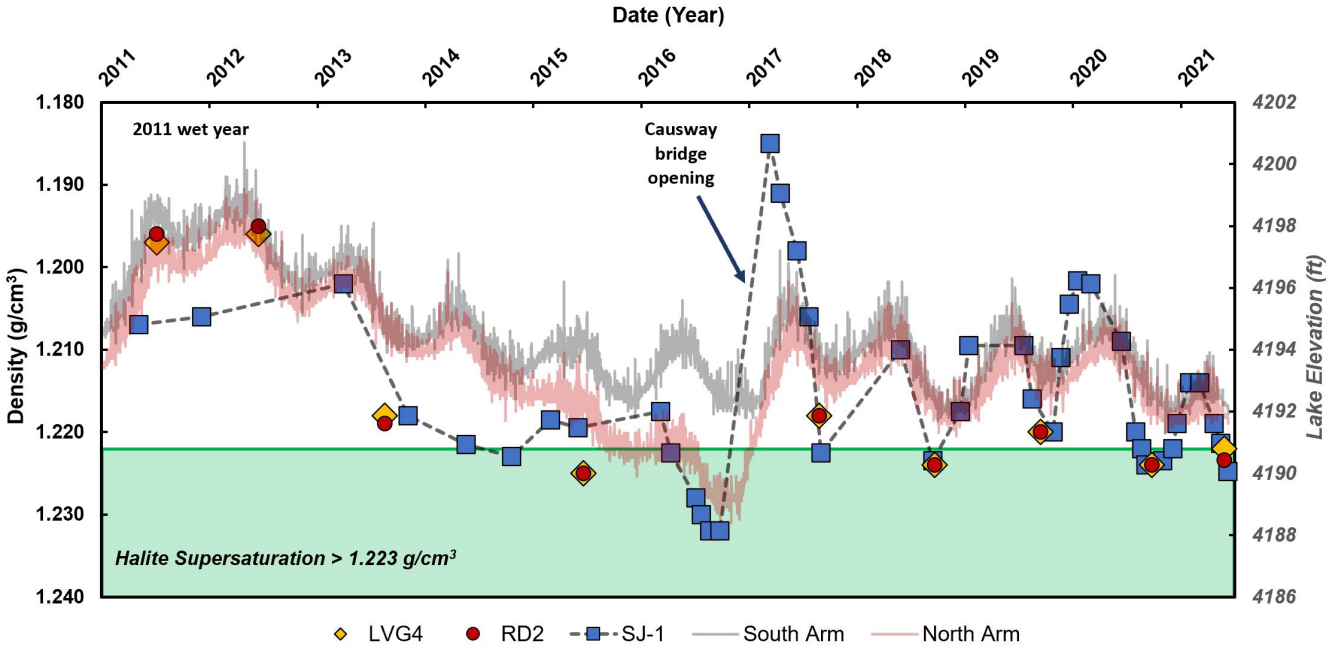

Figure 36. *Density measurements (points, left y-axis, in reverse) over time from the north arm lake sites LVG4, RD2, and SJ-1 superimposed on north and south arm lake elevations (lines, right y-axis) from 2011 to 2021. Density values were measured at room temperature (~20°C) and densities above 1.223 g/cm^3 represent a halite supersaturated lake brine (shaded in green) that corresponds to periods of low lake level. Beginning in 2011, a wet year diluted the brine. From 2012 to 2016 a drought period began and the north arm lake elevation decreased substantially and regained halite saturation from 2015 to December 2016. Following the opening of the causeway breach, dilute inflow waters mixed with north arm waters and the lake became undersaturated with halite. After 2017 to the present, lake elevations for the south and north arms have been in close equilibrium with an offset of ~0.5 ft (south arm is elevated from riverine inflow and lower density). After the opening of the breach, density measurements have corresponded to seasonal changes in lake elevation: lower densities during winter and spring and high lake levels, and high densities during late summer and low lake level. As lake levels have continued to drop, halite saturation was reached during late 2020 and mid-2021. The formation of mirabilite from cold winter lake temperatures also lowers the density of the lake brine and influences the degree of halite saturation.*

but preliminary geochemical modeling and stable isotopes infer that it is a contributing factor for brine evolution. Both spring seeps and mudflat groundwater evolve to north arm brine via evaporation. The origin, residence time, and discharge for groundwater inflow is an ongoing investigation adjoining the north arm, as well as within the lake, and may be more significant for controlling solute balance than previously thought. During higher lake levels, storm surges, and runoff, groundwater solutes that have been sequestered along the mudflats and as chemical precipitates may be recycled into the lake. In addition, we observed halite dissolution features along a part of the lake floor likely caused by subaqueous groundwater discharge and in the nearshore where subaerial halite crusts are partially dissolved around spring seep holes. The extent or amount of groundwater discharge occurring within the lake or in the nearshore and its role for supplying solutes and cycling dissolved NaCl remains unknown.

The formation of mirabilite during cold winter lake temperatures has a seasonal effect on halite saturation. Based on simple lab measurements and density measurements of a north arm brine at 0°C, mirabilite precipitation decreased salinity by ~2%. This suggests that the salinity of the north arm brine should decrease as mirabilite precipitates during the winter, and as lake waters warm during the spring/summer, the salinity of the lake should increase as mirabilite dissolves. The white chemical sediment that we observed coating the lake floor and within the water column upon warmer seasons could partially be a residual of thenardite, the dehydration/dissolution phase of mirabilite. The precipitation and dissolution of mirabilite, coupled with our other observations, implies an opposite halite focusing model compared to the Dead Sea in that the north arm only reaches halite saturation during high evaporative concentration periods in the summer and fall months. We have yet to document the north arm water column and lake bottom during winter to confirm possible lake-wide mirabilite precipitation and the full impact mirabilite may have on halite saturation; however, observations from the nearshore indicate that significant halite dissolution can occur during the cold winter months. Additional work is also needed to determine the relative importance of fresher south arm inflow versus mirabilite precipitation in causing north arm undersaturation during the winter and spring.

ACKNOWLEDGMENTS

This research was funded in part by the Utah Division of Forestry, Fire and State Lands. We thank Jim Van Leeuwen for field assistance on the Utah Division of Wildlife Resources boat and for loaning an inflatable raft to use in the north arm. We thank Nadav Lensky, Ido Sirota, and Ziv Mor for discussions on field work strategies. This publication was improved by constructive comments and helpful reviews by Tim K. Lowenstein, Mike Vanden Berg, Stephanie Carney, Mike Hylland, and Bill Keach.

We would also like to specially acknowledge J. Wallace (Wally) Gwynn, a former UGS scientist who spent a career studying Great Salt Lake. Our work, as well as others' work, at Great Salt Lake builds upon a foundation of research done by Wally. We are grateful for his many contributions.

REFERENCES

Adams, T.C., 1964, Salt migration to the northwest body of Great Salt Lake, Utah: Science, v. 143, no. 3610, p. 1027–1029.

Anati, D.A., 1997, The hydrography of a hypersaline lake *in* Niemi, T., Ben-Avraham, Z., and Gat, J.R., editors, The Dead Sea. The lake and its setting: Oxford University Press, New York, pp. 89–1003.

Anderson, R.B., Naftz, D.L., Day-Lewis, F.D., Henderson, R.D., Rosenberry, D.O., Stolp, B.J., and Jewell, P., 2014, Quantity and quality of groundwater discharge in a hypersaline lake environment: Journal of Hydrology, v. 512, p. 177–194.

Arnon, A., Selker, J.S., and Lensky, N.G., 2016, Thermohaline stratification and double diffusion diapycnal fluxes in the hypersaline Dead Sea: Limnology and Oceanography, v. 61, p. 1214–1231.

Arnow, T., and Stephens, J.C., 1975, Groundwater inflow to Great Salt Lake, Utah [abs]: Geological Society of America Abstracts with Programs, 1975 annual meeting, p. 81.

Baskin, R.L., and Turner, J., 2006, Bathymetric map of the north part of Great Salt Lake, Utah, 2006: U.S. Geological Survey Scientific Investigations Map 2954, 1 plate.

Bowen, B.B., Kipnis, E.L., and Raming, L.W., 2017, Temporal dynamics of flooding, evaporation, and desiccation cycles and observations of salt crust area change at the Bonneville Salt Flats, Utah: Geomorphology, v. 299, p. 1–11.

Cole, D.R., 1982, Tracing fluid sources in the East Shore Area, Utah: Ground Water, v. 20, p. 586–592.

Dames and Moore, undated, Drill logs from the 1974–1975 Great Salt Lake soil boring program: unpublished report for Amoco Production Company, unpaginated.

Genkinger, S., and Putnis, A., 2007, Crystallization of sodium sulfate: supersaturation and metastable phases: Environmental Geology, v. 52, p. 329–337.

Gilbert, G.K., 1890, Lake Bonneville: U.S. Geological Survey Monograph 1, 438 p.

Goodwin, J.H., 1973, Composition and lithology of the salt crust, North Arm, Great Salt Lake, Utah: unpublished report prepared by the Utah Geological and Mineral Survey, 12 p.

Great Salt Lake Salinity Advisory Committee, 2020, Round robin of methods to estimate the salinity of Great Salt Lake waters: Utah Geological Survey Open-File Report 727, variously paginated, https://doi.org/10.34191/OFR-727.

Gwynn, J.W., 2002, Great Salt Lake, Utah—Chemical and physical variations of the brine and effects of the SPRR causeway, 1966-1996, *in* Gwynn, J.W., editor, Great Salt Lake—an overview of change: Utah Department of Natural Resources Special Publication, p. 87-106.

Gwynn, J.W., 2007, Great Salt Lake brine chemistry database and reports—1966-2006: Utah Geological Survey Open-File Report 485, https://doi.org/10.34191/OFR-485.

Hardie, L.A., 2003, Evaporites, *in* Middleton G.V., editor, Encyclopedia of sediments and sedimentary rocks: Kluwer Academic Publishing, Dordrecht, 585p.

Hurlow, H.A., and Burk, N., 2008, Geology and groundwater chemistry, Curlew Valley, northwestern Utah and south-central Idaho—implications for hydrogeology: Utah Geological Survey Special Study 126, 93 p., https://doi.org/10.34191/SS-126.

Jones, B.J, Naftz, D.L., Spencer, R.J., and Oviatt, C.G., 2009, Geochemical evolution of Great Salt Lake, Utah, USA: Aquatic Geochemistry, v. 15, p. 95–121.

Kirby, S.M., Inkenbrandt, P.C., and Rupke, A., 2019, Mapping groundwater quality and chemistry adjacent to Great Salt Lake, Utah: Utah Geological Survey Open-File Report 699, 19 p., https://doi.org/10.34191/OFR-699.

Loving, B.L., Waddell, K.M., and Miller, C.W., 2000, Water and salt balance of Great Salt Lake, Utah, and simulation of water and salt movement through the causeway: U.S. Geological Survey Water-Resources Investigations Report 00-4221, variously paginated.

Lowenstein, T.K.., and Hardie, L.A., 1985, Criteria for the recognition of salt-pan evaporites: Sedimentology, v. 32, p. 627–644.

Madison, R.J., 1970, Effects of a causeway on the chemistry of the brine in Great Salt Lake, Utah: Utah Geological and Mineralogical Survey Water-Resources Bulletin 14, 52 p., https://doi.org/10.34191/B-14.

Marliacy, P., Solimando, R., Bouroukaba, M., and Schuffenecker, L., 2000, Thermodynamics of crystallization of sodium sulfate decahydrate in H_2O-NaCl-Na_2SO_4—application to $Na_2SO_4 \cdot 10H_2O$-based latent heat storage materials: Thermochimica Acta, v. 344, p. 85–94.

Mills, S.E., Rupke, A., Vanden Berg, M.D., and Boden, T., 2020, Utah mining 2019—Metals, industrial minerals, coal, uranium, and unconventional fuels: Utah Geological Survey Circular 130, 37 p., https://doi.org/10.34191/C-130.

Mohammed, I.N., and Tarboton, D.G., 2012, An examination of the sensitivity of the Great Salt Lake to changes in inputs: Water Resources Research, v. 48, no. W11511, 17 p.

Oviatt, C.G., Currey, D.R., and Sack, D., 1992, Radiocarbon chronology of Lake Bonneville, Eastern Great Basin, USA: Palaeogeography, Palaeoclimatology, Palaeoecology, v. 99, no. 3-4, p. 225–241.

Plummer, L.N., Parkhurst, D.L., Fleming, G.W., and Dunkle, S.A., 1988, A computer program incorporating Pitzer's equations for calculations of chemical reactions in brines: U.S. Geological Survey Water-Resources Investigations Report 88-4153, 310 p.

Rasmussen, M., Dutta, S., Neilson, B.T., and Crookston, B.M., 2021, CFD model of the density-driven bidirectional flow through the West Crack Breach in the Great Salt Lake Causeway: Water, v. 13, no. 17, p. 2423.

Rozanski, K., Araguás-Araguás, L., and Gonfiantini, R., 1993, Isotopic patterns in modern global precipitation, *in* Swart, P.K., Lohman, K.C., Mckenzie, J., and Savin, S., editors, Climate change in continental isotopic record–volume 78: American Geophysical Union, Geophysical Monograph, p. 1–37.

Rupke, A., and Boden, T., 2020, Great Salt Lake north arm salt crust monitoring, spring 2017 update: Utah Geological Survey Open-File Report 714, 13 p., https://doi.org/10.34191/OFR-714.

Rupke, A., Boden, T., and Nielsen, P., 2016, Great Salt Lake's north arm salt crust: Utah Geological Survey Report of Investigation 276, 47 p., 1 plate, https://doi.org/10.34191/RI-276.

Rupke, A., and McDonald, A., 2012, Great Salt Lake brine chemistry database, 1966–2011: Utah Geological Survey Open-File Report 596, 7 p., 1 appendix, https://doi.org/10.34191/OFR-596.

Scott, W.E., McCoy, W.D., Shroba, R.R., and Rubin, M., 1983, Reinterpretation of the exposed record of the last two cycles of Lake Bonneville, Western United States: Quaternary Research, v. 20, no. 3, p. 261–285.

Shope, C.L, and Angeroth, C.E., 2015, Calculating salt loads to Great Salt Lake and the associated uncertainties for water year 2013—updating a 48 year old standard: Science of the Total Environment, v. 536, p. 391–405.

Sirota, I., Enzel, Y., and Lensky, N.G., 2017, Temperature seasonality control on modern halite layers in the Dead Sea—in situ observations: Geological Society of America Bulletin, v. 129, p. 1181–1194.

Smoot, J.P., and Lowenstein, T.K., 1991, Depositional environments of non-marine evaporites: Developments in Sedimentology, Elsevier, p. 189–347.

Spencer, R.J., Eugster, H.P., and Jones, B.F., 1985, Geochemistry of Great Salt Lake, Utah I—hydrochemistry since 1850: Geochimica et Cosmochimica Acta, v. 49, p. 727–737.

Stewart K.M., Walker, K.F., and Likens, G.E., 2009, Meromictic lakes–volume 2, *in* Likens, G.E., editor, Encyclopedia of Inland Waters: Oxford, Elsevier, p. 589–602.

Utah Geological Survey, 2020, Great Salt Lake brine chemistry database: Online, https://geology.utah.gov/docs/xls/GSL_brine_chem_db.xlsx, accessed June 2021.

Woodhall, R.J., 1980, Engineering problems of Great Salt Lake, Utah, marine oil drilling operation, *in* Gwynn, J.W., editor, Great Salt Lake—a scientific, historical and economic overview: Utah Geological and Mineral Survey Bulletin 116, p. 377–392, https://doi.org/10.34191/B-116.

APPENDIX A:

Nearshore Salt Crust Observations

Link to supplemental data download:
https://ugspub.nr.utah.gov/publications/reports_of_investigations/ri-283/ri-283-a.pdf

APPENDIX B:

Nearshore Salt Crust Thickness Measurements

Link to supplemental data download:
https://ugspub.nr.utah.gov/publications/reports_of_investigations/ri-283/ri-283-b.pdf

APPENDIX C:

Supplementary Underwater Images

Link to supplemental data download:
https://ugspub.nr.utah.gov/publications/reports_of_investigations/ri-283/ri-283-c.pdf

APPENDIX D:

Saturation Tests of North Arm Brine

Link to supplemental data download:
https://ugspub.nr.utah.gov/publications/reports_of_investigations/ri-283/ri-283-d.pdf